Severed Molecules Functionally Define the Boundaries of the Cystic Fibrosis Transmembrane Conductance Regulator's NH_2-terminal Nucleotide Binding Domain

Kim W. Chan,* László Csanády,* Donna Seto-Young,* Angus C. Nairn,‡ and David C. Gadsby*

From the *Laboratory of Cardiac/Membrane Physiology, and ‡Laboratory of Molecular and Cellular Neuroscience, The Rockefeller University, New York, New York 10021

abstract The cystic fibrosis transmembrane conductance regulator is a Cl^- channel that belongs to the family of ATP-binding cassette proteins. The CFTR polypeptide comprises two transmembrane domains, two nucleotide binding domains (NBD1 and NBD2), and a regulatory (R) domain. Gating of the channel is controlled by kinase-mediated phosphorylation of the R domain and by ATP binding, and, likely, hydrolysis at the NBDs. Exon 13 of the CFTR gene encodes amino acids (aa's) 590–830, which were originally ascribed to the R domain. In this study, CFTR channels were severed near likely NH_2- or COOH-terminal boundaries of NBD1. CFTR channel activity, assayed using two-microelectrode voltage clamp and excised patch recordings, provided a sensitive measure of successful assembly of each pair of channel segments as the sever point was systematically shifted along the primary sequence. Substantial channel activity was taken as an indication that NBD1 was functionally intact. This approach revealed that the COOH terminus of NBD1 extends beyond aa 590 and lies between aa's 622 and 634, while the NH_2 terminus of NBD1 lies between aa's 432 and 449. To facilitate biochemical studies of the expressed proteins, a Flag epitope was added to the NH_2 termini of full length CFTR, and of CFTR segments truncated before the normal COOH terminus (aa 1480). The functionally identified NBD1 boundaries are supported by Western blotting, coimmunoprecipitation, and deglycosylation studies, which showed that an NH_2-terminal segment representing aa's 3–622 (Flag3-622) or 3–633 (Flag3-633) could physically associate with a COOH-terminal fragment representing aa's 634–1480 (634-1480); however, the latter fragment was glycosylated to the mature form only in the presence of Flag3-633. Similarly, 433-1480 could physically associate with Flag3-432 and was glycosylated to the mature form; however, 449-1480 protein seemed unstable and could hardly be detected even when expressed with Flag3-432. In excised-patch recordings, all functional severed CFTR channels displayed the hallmark characteristics of CFTR, including the requirement of phosphorylation and exposure to MgATP for gating, ability to be locked open by pyrophosphate or AMP-PNP, small single channel conductances, and high apparent affinity of channel opening by MgATP. Our definitions of the boundaries of the NBD1 domain in CFTR are supported by comparison with the solved NBD structures of HisP and RbsA.

key words: adenosine triphosphate-binding cassette transporter • domain structure • chloride channel • gating kinetics • coimmunoprecipitation

INTRODUCTION

The cystic fibrosis transmembrane conductance regulator is the ~170-kD protein product of the gene mutated in cystic fibrosis patients (Riordan et al., 1989). The topological organization of CFTR that was predicted from the nucleotide sequence when the gene was cloned (Riordan et al., 1989) has largely stood the test of time. CFTR comprises two approximately homologous halves, each incorporating a putative hexahelical transmembrane domain followed, in the linear sequence, by a cytoplasmic nucleotide binding domain (NBD).[1] The two halves are linked by a charged, cytoplasmic, ~200-residue regulatory (R) domain that contains multiple sites for phosphorylation by protein kinase A and protein kinase C (Riordan et al., 1989). Apart from this large linker domain, CFTR's overall predicted domain structure identifies it as a member of the very large family of ATP-binding cassette (ABC) membrane transporters (e.g., Higgins, 1992). There are several other well-known eukaryotic ABC proteins such as P-glycoprotein (Pgp) and multi-drug resistance-related protein (MRP), both associated with multi-drug resistance in tumor cells, and STE6, the **a**-mating factor transporter of yeast. In all these examples, both mem-

Address correspondence to David C. Gadsby, Laboratory of Cardiac/Membrane Physiology, The Rockefeller University, 1230 York Avenue, New York, NY 10021-6399. Fax: 212-327-7589; E-mail: gadsby@rockvax.rockefeller.edu

[1]*Abbreviations used in this paper:* aa, amino acid; ABC, ATP-binding cassette; ER, endoplasmic reticulum; MRP, multi-drug resistance-related protein; NBD, nucleotide binding domain; Pgp, P-glycoprotein; PP_i, pyrophosphate; R domain, regulatory domain.

brane-spanning domains and the two NBDs are encoded by a single large gene. But, in the much larger number of prokaryotic ABC transporters, the NBDs are frequently expressed from individual genes (as for HisP, the NBD of histidine permease; e.g., Hung et al., 1998), or two NBDs may be fused in a single gene product (as for RbsA, the NBDs of the ribose transporter; e.g., Armstrong et al., 1998), while the transmembrane domains may be expressed from yet other genes. One implication of such post-translational assembly of functional transporters in bacteria is that these separate gene products (which, in many cases, are single domains) must each possess all the information needed to fold correctly and to interact with the complementary domains that make up a fully functioning transporter.

Unlike any other ABC protein, CFTR functions as a chloride channel (reviewed in Sheppard and Welsh, 1999). The R domain, with its multiple phosphorylation sites, is also unique to CFTR, and in its dephosphorylated state it prevents the opening of CFTR Cl^- channels. Even once it has been phosphorylated by PKA, however, a CFTR channel cannot open until it is exposed to ATP or another hydrolyzable nucleoside triphosphate. The regulation of opening and closing of CFTR channels by phosphorylation of the R domain and nucleotide binding and hydrolysis at the NBDs is extremely complex and is not yet fully understood. One suggestion is that ATP hydrolysis at NBD1 results in both channel opening and binding of ATP at NBD2, which then stabilizes the open-channel conformation (e.g., Csanády and Gadsby, 1999; Gadsby and Nairn, 1999). Recently, however, on the basis of direct comparisons of ATP hydrolysis and gating measurements of wild type and mutant CFTR, it has been suggested that ATP hydrolysis might not be strictly coupled to channel opening (Ramjeesingh et al., 1999). Still, it remains clear that interactions between the two NBDs, and between the NBDs and the R domain, play important roles in the gating of CFTR channels (reviewed in Csanády and Gadsby, 1999; Gadsby and Nairn, 1999; Sheppard and Welsh, 1999).

Further dissection of these roles would greatly benefit from structural information on each of these domains, which is presently lacking. Nevertheless, peptide models of the R domain (Picciotto et al., 1992; Dulhanty and Riordan, 1994), of the NH_2-terminal NBD (NBD1; Hartman et al., 1992; Ko and Pedersen, 1995; Yike et al., 1996; Ko et al., 1997; Clancy et al., 1998), and of the COOH-terminal NBD (NBD2; Randak et al., 1996, 1997) have been expressed and partly characterized. A valid concern with several of these constructs is the sparse knowledge of the location of the domain boundaries. As a first step towards addressing this concern, we attempted to define the boundaries of NBD1 of CFTR by exploiting a functional approach. It has already been shown that the CFTR channel protein can be severed near the COOH-terminal end of the R domain, and the two halves coexpressed to form a functional complex (Ostedgaard et al., 1997). Therefore, given the modular design of ABC transporters in general, we reasoned that judicious cuts in the links flanking NBD1 ought to be tolerated. Indeed, cuts between three of the four domains of STE6 did not abrogate its function (Berkower et al., 1996). We describe here our search for the boundaries of NBD1 by coexpressing contiguous, or near contiguous, segments of CFTR in *Xenopus* oocytes and assessing function with two-microelectrode voltage clamp and excised-patch recordings. Expression and physical association of the CFTR protein segments were assayed using immunoblots and coimmunoprecipitation. Using this approach, we find that the NH_2 terminus of NBD1 lies between amino acids (aa) 432 and 449 and the COOH terminus lies between aa's 622 and 634. Moreover, regions spanning aa's 415–432 and 634–667 can be omitted without severely impairing CFTR channel function.

MATERIALS AND METHODS

Molecular Biology

pGEMHE-WT was constructed by subcloning a CFTR cDNA fragment, excised from pBQ4.7 (a gift from Dr. Johanna Rommens, The Hospital for Sick Children, Toronto, Ontario, Canada), into the SmaI and XhoI (BioLabs, Inc.) sites of pGEMHE (Liman et al., 1992). A Flag epitope (M-DYKDDDDK) followed by a leucine was added to the NH_2 terminus of a CFTR fragment containing amino acids 3–835 by running two consecutive PCR reactions using a GeneAmp PCR system 2400 (PerkinElmer). In the first PCR reaction, FlagFW1 (5′-TACAAAGACGACGACGACAAGCTTAGGTCGCCTCTGGAAAAGGC) and 835RV (5′-CCG*CTCGAG*CTAATCAAAAAAGCACTCCTTTAAGTC) were used with pGEMHE-WT as template. In the second PCR reaction, FlagFW2 (5′-TCC*CCCGGG*CCGCCATGGATTACAAAGACGACGACGACAAG) and 835RV were used with the purified PCR product, obtained from the first reaction, as template. The PCR product from the second reaction was subcloned into the SmaI and XhoI sites of pGEMHE to make pGEMHE-Flag3-835. pGEMHE-Flag3-589 was made by PCR using T7 FW primer (5′-TAATACGACTCACTATAGGGCGAATT) and a specific reverse oligonucleotide primer 589RV (5′-CCG*CTCGAG*CTAGCTTTCAAATATTTCTTTTTC) with pGEMHE-Flag3-835 as template, followed by subcloning into pGEMHE. pGEMHE-Flag3-611, pGEMHE-Flag3-622, pGEMHE-Flag3-633, pGEMHE-Flag3-432, and pGEMHE-Flag3-414 were similarly constructed using T7 FW and the corresponding specific reverse primers. pGEMHE-590-1480 was made by PCR using 590FW (5′-TCC*CCCGGG*CCGCCATGTGTCTGTAAACTGA-TGGCTAACAAAA) and SP6 RV (5′-CGCCAAGCTATTTAGGTGACACTATAG) with pGEMHE-WT as template followed by subcloning. pGEMHE-449-1480, pGEMHE-433-1480, pGEMHE-634-1480, and pGEMHE-668-1480 were similarly constructed using specific forward primers. pGEMHE-FlagWT was constructed by subcloning a BspEI/XhoI fragment from pGEMHE-WT, which encodes part of TM6 and all the domains that follow, into BspEI and XhoI sites of pGEMHE-Flag3-835. pGEMHE-1-432 and pGEMHE-1-633 were constructed by PCR reactions using pGEMHE-WT as template. All PCR reactions used Pfu polymerase (Stratagene) and a

low number (15–20) of PCR cycles, and all constructs were confirmed by automated sequencing. The coding sequence for every engineered CFTR segment began with a Kozak consensus sequence (CCGCCATG) that includes the methionine start codon. Plasmid DNAs were linearized with NheI, and cRNAs were produced by in vitro transcription using a T7 mMessage mMachine kit (Ambion), and then run on denaturing gels to check size and quality. RNA concentration was estimated by comparison with a known amount of 0.24–9.5 kb RNA ladder (GIBCO BRL).

Isolation and Injection of Xenopus Oocytes

Stage V–VI oocytes were isolated from adult female *Xenopus laevis* (Nasco) by partial ovariectomy under Tricaine (1% solution) anaesthesia and were defolliculated by treatment at room temperature (21–23°C) for up to 2 h, with ~2 mg/ml collagenase (Type II; Worthington Biochemicals or Type I; GIBCO BRL) in nominally Ca^{2+}-free oocyte Ringer's solution containing (mM): 82.5 NaCl, 2 KCl, 1 $MgCl_2$, 5 HEPES, pH 7.5). Defolliculated oocytes were rinsed extensively with Ca^{2+}-free Ringer's (three to five washes, 50-ml each), and then incubated at 18°C for several hours in Ringer's with 1.8 mM Ca^{2+} and 50 μg/ml gentamycin (GIBCO BRL) before they were pressure-injected (nanojet; Drummond Scientific) with cRNAs. Injection pipettes were pulled (PP83; Narishige) from glass capillaries (3-000-203-G/X; Drummond Scientific) and their tips were broken to an internal diameter of 10–20 μm. Usually, and unless otherwise specified, 2.5 ng of each cRNA, premixed if for coexpression, in a constant total volume of 50 nl, were injected per oocyte. Injected oocytes were further incubated at 18°C for 2–3 d before they were used for recording or for preparation of membranes.

Electrophysiology

For two-microelectrode voltage-clamp measurements, oocytes in a plexiglass recording chamber (volume ~150 μl) were continuously superfused (~2 ml/min) at ~22°C with gravity-fed solutions selected by manual valves (Hamilton). The dead volume was ~100 μl, and solutions were completely exchanged in <8 s. The standard bath solution was Ca^{2+}-free Ringer's solution. The chamber was connected to virtual ground circuitry through Ag/AgCl electrodes in 2.5% agar/3 M KCl bridges. Currents were measured by a voltage-clamp amplifier (OC-725A oocyte clamp; Warner Instrument Corp.), filtered at 50 Hz by an eight-pole Bessel filter (Frequency Devices, Inc.), digitized online at 100 Hz using a Digidata 1200 board (Axon Instruments, Inc.) with pCLAMP 6.0.2 software (Axon Instruments, Inc.), and stored on disk. Microelectrodes, pulled from glass capillaries (3-000-210-G; Drummond Scientific), were filled with 3 M KCl and had resistances of 0.5–2 MΩ. Voltage steps were applied via the amplifier's toggle switch (duration 0.5–1 s) or using pCLAMP software. Steady state currents were averaged over 200 ms near the ends of 1-s voltage steps, and plotted against voltage. Conductance was calculated from linear fits to the steady currents between −60 and −20 mV. Average values were from at least five oocytes.

For patch-clamp recording, oocytes were shrunk for ~2 min in standard bath solution containing (mM): 138 NMG, 2 Mg-sulfamate, 5 HEPES, 0.5 EGTA, 134 sulfamic acid, pH 7.1 with sulfamic acid, supplemented with 100 mM NaCl. The vitelline membranes were removed manually and the oocytes were transferred to a recording chamber containing standard bath solution. Patch pipettes were pulled from borosilicate glass (N-51A; Drummond Scientific) using a vertical pipette puller, and fire-polished to a tip diameter of 1–2 μm (4–7 MΩ). The pipette solution contained (mM): 138 NMG, 2 $MgCl_2$, 5 HEPES, 136 HCl, pH 7.4 with HCl. 200–300-GΩ seals were obtained by gentle suction. Patches were excised and transferred to a flow chamber, where the cytoplasmic surface was continuously superfused at 21–23°C with standard bath solution containing various test substances. Switching between solutions was implemented by computer-driven electric valves (General Valve Corp.). With the dead volume of ~20 μl and flow rate of ~0.5 ml/min, complete solution exchange took 2–4 s. Solution-exchange rate was verified at the end of each recording by applying a brief pulse of 2 mM Ca-sulfamate, and observing the rate of decay of endogenous Ca^{2+}-activated Cl^--channel current upon Ca^{2+} removal. The bath electrode (Ag/AgCl pellet in 100 mM KCl) was connected to the flow chamber by an agar bridge (4% agar in 100 mM KCl). Outward unitary currents in CFTR channels were recorded at a pipette potential of −40 mV (V_m = +40 mV) via an Axopatch 200A amplifier (Axon Instruments, Inc.), filtered at 100 Hz with an eight-pole Bessel filter (Frequency Devices, Inc.), digitized online at 1 kHz using an ITC-16 board (Instrutech) and recorded on disk by PULSE software (Heka Elektronik). CFTR channels were activated by 300 nM catalytic subunit of protein kinase A purified from bovine heart (Kaczmarek et al., 1980); measurements of steady state macroscopic CFTR current at various [PKA] (Csanády et al., 1998) showed that even 300 nM was less than saturating due to highly active membrane-associated phosphatases. MgATP (Sigma-Aldrich) was added from a 400-mM stock solution (pH 7.2 with NMG). At the end of each experiment, channels were counted by locking them in the open state with 2 mM NMG-pyrophosphate (PP_i; Fluka) in the presence of 100 μM MgATP and 300 nM PKA, supplemented by 2 mM Mg-sulfamate (for example, see Fig. 8, below). Li_4-AMPPNP (Sigma-Aldrich) was added from a 400-mM stock solution.

For kinetic analysis, digitized (100 Hz bandwidth, 1 kHz sampling rate), baseline-corrected currents from records containing one to seven channels were idealized using conventional half-amplitude threshold crossing. The desired parameters were mean burst and interburst durations for the intact and severed CFTR constructs, and these were determined as follows. First, gating transitions were modeled as a simple closed–open scheme, while brief ("flickery") closures were attributed to pore blockage events (e.g., Ishihara and Welsh, 1997), resulting in the three-state closed–open-blocked scheme:

$$C \underset{r_{OC}}{\overset{r_{CO}}{\rightleftharpoons}} O \underset{r_{BO}}{\overset{r_{OB}}{\rightleftharpoons}} B \qquad \text{(SCHEME I)}$$

Then, for each record, the best set of rate constants, r_{CO}, r_{OC}, r_{OB}, and r_{BO}, was extracted from a simultaneous maximum likelihood fit to the dwell-time histograms obtained from all of the conductance levels, as described (Csanády, 2000). Finally, mean interburst durations were calculated using the relationship $\tau_{ib} = 1/r_{CO}$, while mean burst durations were given by $\tau_b = (1/r_{OC})(1 + r_{OB}/r_{BO})$. As a control, because a similar burst-type gating to that of the C-O-B scheme arises from the alternative linear three-state model, closed–closed–open (C-C-O), the events list was sometimes also fitted assuming this C-C-O scheme; this yielded a new set of rate constants, but identical mean burst and interburst durations for the same record in every case. Open probabilities (P_o) were calculated directly from the events lists as the time average of the idealized current divided by channel number (estimated for each patch as described above) and the measured single-channel current amplitude.

Macroscopic currents from patches containing 20–1,000 CFTR channels were digitally refiltered at 10 Hz using a Gaussian filter, and then sampled at 50 Hz. The average steady state current towards the end of 10–30-s test applications of 50 μM MgATP was

normalized to the mean of the steady currents at 2 mM MgATP before and after the test, and the ratios were used to estimate apparent affinities for ATP.

Single-channel conductances were estimated from amplitude histograms of excised-patch currents recorded at holding potentials of −80, −40, 0, +40, and +80 mV, in symmetrical 140 mM [Cl^-]. The distances between adjacent peaks, from fits to sums of Gaussians, were plotted against voltage, and straight lines fitted to yield conductances. Results are presented as mean ± SEM of five or more experiments for kinetic data, and three or more experiments for apparent affinities and single-channel conductances. Statistical significances were evaluated by Student's *t* test.

Preparation of Oocyte Membranes

Oocytes injected with cRNA were incubated for 48 h, and then frozen in liquid nitrogen and stored at −80°C. Aliquots of ~150 frozen oocytes were homogenized at 4°C with 1 ml lysis buffer, containing (mM): 10 HEPES, pH 7.5 with NaOH, 6 EDTA, 50 NaCl, 1 mg/ml BSA, 1 PMSF, and protease inhibitor cocktail (Calbiochem; final concentrations were 1 mM AEBSF HCl, 300 nM aprotinin, 2 μM E-64, 2 μM leupeptin hemisulfate), and the suspensions were centrifuged at 3,000 *g* for 10 min. Supernatants were kept and centrifuged again at 3,000 *g* for 10 min. 2 ml of lysis buffer was added to the resulting supernatants before centrifugation at 173,600 *g* for 1 h. The pellets were washed with 3 ml modified lysis buffer (with 10% glycerol instead of BSA, and only 0.5 mM PMSF), the centrifugation was repeated and the pelleted membranes resuspended in 0.2 ml modified lysis buffer and stored at −80°C.

Western Blotting and Coimmunoprecipitation

Membrane proteins (75 μg total membrane protein per lane) were resolved by 7.5% SDS-PAGE and blotted onto nitrocellulose membranes using a semi-dry transfer cell (Bio-Rad Laboratories). Protein bands containing the R domain were detected with anti–R-domain Ab (Picciotto et al., 1992) and horseradish perozidase–conjugated goat anti–rabbit IgG as the secondary Ab. NH_2-terminal fragments were detected either using anti–Flag M2 monoclonal Ab (Sigma-Aldrich) with HP-conjugated goat anti–mouse IgG as the secondary Ab or, in coimmunoprecipitation experiments, using an anti–NH_2-terminal Ab (A_2; kindly provided by Dr. W. Skach, Oregon Health Sciences University, Portland, OR) with HP-conjugated goat anti–rabbit IgG as secondary Ab. Protein bands were visualized with the ECL Western blotting kit (Amersham Pharmacia Biotech).

Coimmunoprecipitation was by a procedure modified from that of Ostedgaard et al. (1997). 450 μg of each total membrane protein sample were solubilized for 1 h in 1 ml solubilization buffer (1.25% digitonin, 150 mM NaCl, 50 mM Tris/HCl, pH 7.5) and the suspensions centrifuged at 173,600 *g* for 1 h. Each supernatant of soluble proteins was mixed with 200 μl of anti–Flag M2 affinity gel (Sigma-Aldrich) prewashed with solubilization buffer, and the mixtures were rocked overnight, and then centrifuged at 26,000 *g* for 5 min. The pellets, containing anti–Flag M2 affinity gel with bound proteins, were washed three times with solubilization buffer, three times with high-salt buffer (500 mM NaCl, 50 mM Tris/HCl, pH 7.5), and then twice with 50 mM Tris, pH 7.5. The coimmunoprecipitated proteins were eluted with 150 μl Laemmli buffer.

Deglycosylation and Protein Determination

Oocyte membrane protein samples (75 μg) were treated with *N*-glycosidase-F and endoglycosidase-H for 1 h at 37°C following the supplier's protocol (Boehringer). Protein concentrations were measured with bicinchonic acid (Pierce Chemical Co.).

RESULTS

Wild-Type CFTR Channels Display Basal Activity in Resting Xenopus Oocytes

Xenopus oocytes have proven to be a convenient expression system for functional and biochemical analysis of a variety of ion channels, including CFTR (e.g., Bear et al., 1991; Smit et al., 1993; Wilkinson et al., 1996; Naren et al., 1999), and were adopted for this study. Fig. 1, A–C, shows typical recordings of membrane current in oocytes, held near their resting potentials, 2 d after injecting them with (A) water, (B) WT CFTR cRNA, or (C) a mixture of two cRNAs encoding contiguous CFTR segments Flag3-633 and 634-1480. Membrane conductance was monitored every minute or so with ±60-mV steps away from the holding potential, which yielded negligibly small currents (±0.1 μA or less) at all times in control, H_2O-injected oocytes (also in uninjected oocytes). By contrast, these voltage steps elicited clearly discernible currents of approximately ±1 μA in unstimulated oocytes expressing WT CFTR (reflecting their mean basal conductance, 10 ± 1 μS) and of approximately ±10 μA (mean activated conductance, 173 ± 4 μS) within ~2 min of stimulating the cAMP/PKA pathway in those oocytes by exposing them to 50 μM forskolin plus 1 mM IBMX (Fig. 1 and Table I). The steady current levels near the ends of 1-s voltage pulses to potentials between −100 and +80 mV are shown in the steady state current–voltage plots in Fig. 1 D. For oocytes expressing WT CFTR, these I-V relationships were approximately linear, and showed roughly the same reversal potential, both before and during stimulation of PKA (Fig. 1 D, c and d). In oocytes expressing WT CFTR, but not in uninjected oocytes, subsequent injection of the PKA inhibitor RpcAMPS (estimated final concentration, ~1 mM) diminished the basal conductance until it matched that of H_2O-injected, or of uninjected, oocytes (Csanády, L., K.W. Chan, D. Seto-Young, D.C. Kopsco, A.C. Nairn, and D.C. Gadsby, manuscript submitted for publication). This indicates that the basal conductance reflected activity of WT-CFTR channels phosphorylated by basally active PKA, and that phosphatases must also have been constitutively active in the oocytes to dephosphorylate CFTR channels and abolish their basal activity after introduction of RpcAMPS. Accordingly, the forskolin- and IBMX-induced increase in membrane conductance of oocytes expressing CFTR presumably reflected activation of CFTR by PKA-mediated phosphorylation (e.g., Bear et al., 1991; Smit et al., 1993) and possibly also a direct stimulation of CFTR by IBMX (Al-Nakkash and Hwang, 1999).

Defining the COOH-terminal Boundary of NBD1 by Assessing Function of Coexpressed Severed CFTR Segments

The location of the boundary between NBD1 and the R domain in CFTR is presently unclear. The initial sugges-

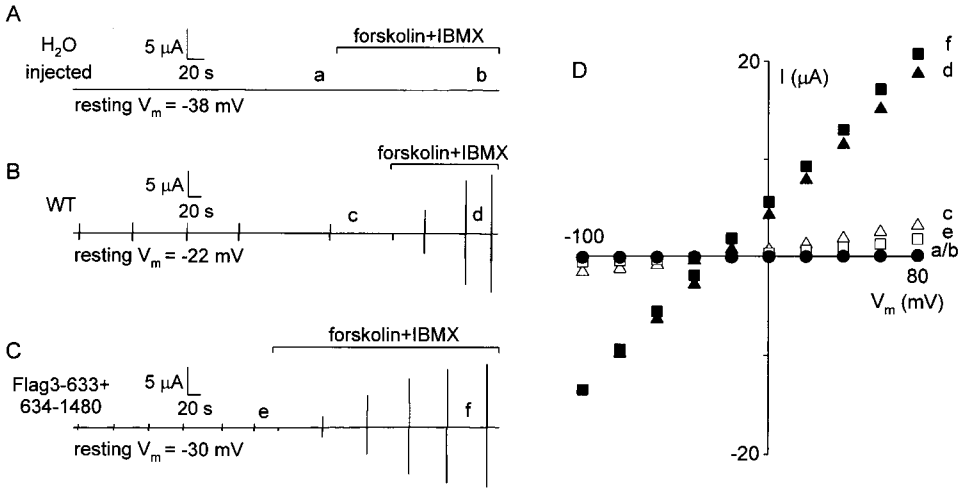

Figure 1. (A–C) Representative current recordings from oocytes held at their initial resting membrane potential in Ca^{2+}-free oocyte Ringer's solution. Oocytes were injected with (A) water, (B) 6 ng of WT CFTR RNA, or (C) 2.5 ng of Flag3-633 RNA plus 2.5 ng 634-1480 RNA. Horizontal bars mark periods of exposure to 50 μM forskolin plus 1 mM IBMX. Basal and activated conductances were monitored by applying ±60-mV voltage steps ≤1-s long. Magnitudes of basal and activated conductances and rates of activation were similar in oocytes injected with 2.5 or 6 ng of WT CFTR RNA. (D) I-V relationships obtained at times a-f in A–C; empty symbols, resting (basal); filled symbols, activated. Steady current levels averaged over ~200 ms near the end of 1-s voltage steps from −100 to +80 mV, in 20-mV increments, are plotted against voltage.

tion was that exon 13 of CFTR, comprising aa's 590–830, encoded the R domain, and hence that the exon 12/13 junction marked the boundary between NBD1 and the R domain (Riordan et al., 1989). If that were so, it might reasonably be expected that functional CFTR channels could be reconstituted by coexpression of the two contiguous segments of CFTR severed between residues 589 and 590; i.e., Flag3-589 plus 590-1480. The NH_2-terminal Flag epitope was incorporated to facilitate immunoprecipitation and detection of the expressed proteins (see below). Injection of oocytes with a mixture of the two cRNAs encoding these two segments resulted in conductances that were negligible under both basal (2 ± 1 μS) and activated (2 ± 1 μS) conditions, just as in control, uninjected oocytes (Fig. 2 and Table I). On the assumption that NBD1 likely stretches beyond aa 589 (compare Annereau et al., 1997), a series of constructs was made in which the COOH terminus of Flag3-589 was incrementally extended. Each of these constructs in turn was coexpressed with the 590-1480 segment, and basal and activated conductances were measured to assess channel function (Fig. 2). These conductances mimicked those of uninjected oocytes until the Flag-tagged CFTR segment was extended to aa 633. Thus, basal and activated conductances were 2 ± 1 and 3 ± 1 μS for oocytes injected with Flag3-622 plus 590-1480, but jumped to 8 ± 1 and 91 ± 7 μS in oocytes coexpressing Flag3-633 plus 590-1480. However, the basal and activated conductances produced by Flag3-633 plus 590-1480 constructs were both smaller than those attained by WT CFTR (Fig. 2). Speculating that this shortfall might be attributable to the repetition of residues 590 to 633 upon coexpression of Flag3-633 plus 590-1480, we removed the overlapping residues by coexpressing Flag3-633 with segment 634-1480, and found basal and activated conductances of 17 ± 1 and 182 ± 4 μS, respectively, comparable with those of oocytes expressing WT CFTR (Figs. 1, B–D, and 2; Table I).

These results show that robust CFTR channel function is obtained when the COOH terminus of the segment Flag3-589 is extended to aa 633 (but not to aa

TABLE I

Conductances of Oocytes Expressing Various CFTR Constructs

Construct	Basal conductance	*n*	Activated conductance	*n*
Uninjected	3 ± 0.3	21	2 ± 0.2	34
WT (1-1480)	10 ± 1	16	173 ± 4	37
Flag3-414	2 ± 1	5	3 ± 0.2	5
Flag3-432	4 ± 0.4	8	3 ± 0.4	8
Flag3-589	3 ± 0.3	5	3 ± 0.4	5
Flag3-611	1 ± 0.1	5	2 ± 0.1	5
Flag3-622	1 ± 0.1	5	2 ± 0.1	5
Flag3-633	3 ± 1	14	2 ± 0.2	15
433-1480	4 ± 1	14	2 ± 0.2	10
449-1480	2 ± 0.3	5	1 ± 0.2	5
590-1480	4 ± 0.4	5	3 ± 0.5	8
634-1480	4 ± 1	9	5 ± 1	10
668-1480	3 ± 0.3	5	3 ± 0.3	5
Flag3-589+590-1480	2 ± 1	6	2 ± 0.4	13
Flag3-611+590-1480	2 ± 1	8	3 ± 0.3	14
Flag3-622+590-1480	2 ± 0.3	5	3 ± 0.4	9
Flag3-633+590-1480	8 ± 1	11	91 ± 7	21
Flag3-633+634-1480	17 ± 1	9	182 ± 4	11
Flag3-622+634-1480	1 ± 0.1	5	1 ± 0.1	5
Flag3-633+668-1480	16 ± 1	8	175 ± 7	8
Flag3-589+449-1480	2 ± 0.2	5	2 ± 0.2	5
Flag3-589+433-1480	2 ± 0.2	11	129 ± 12	9
Flag3-432+433-1480	6 ± 1	16	157 ± 5	18
Flag3-432+449-1480	3 ± 0.4	9	2 ± 0.2	10
Flag3-414+433-1480	7 ± 1	5	195 ± 5	10

Mean (±SEM) basal and activated membrane conductances (μS) of oocytes injected with cRNAs (2.5 ng) encoding the various CFTR constructs examined. *n*, number of observations.

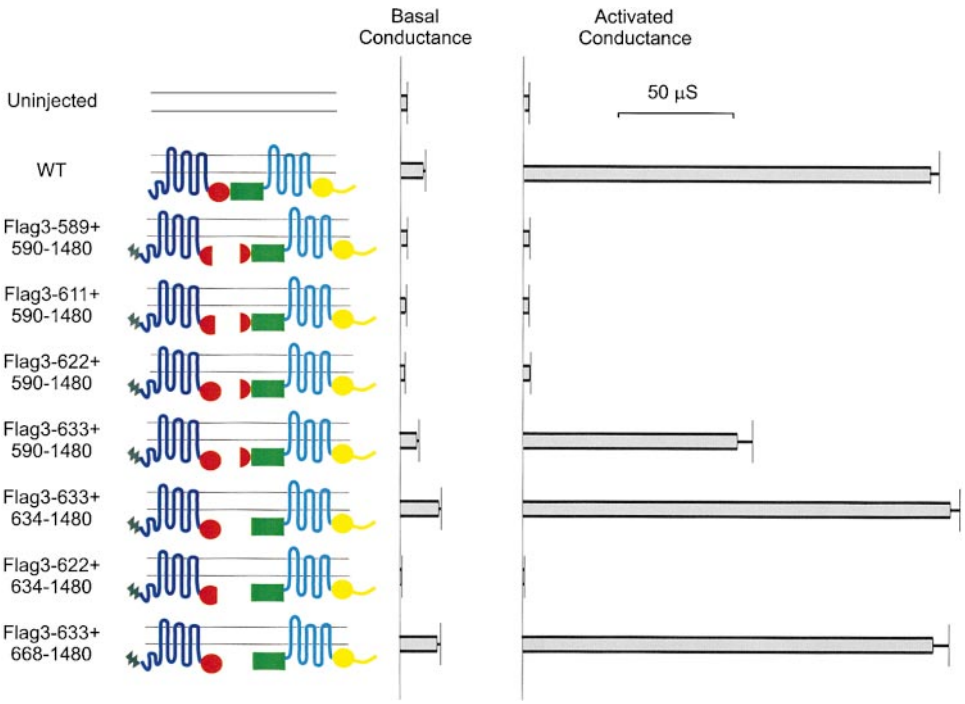

Figure 2. Defining the COOH-terminal boundary of NBD1 by coexpressing severed CFTR segments. Bars show mean (±SEM) basal and activated conductances (by 50 μM forskolin plus 1 mM IBMX) of oocytes injected with cRNAs (2.5 ng per construct) of various CFTR segments cartooned at left: NH_2-terminal Flag epitope (black zigzag); transmembrane domains (blue, cyan); NBD1 (red); R domain (green); NBD2 (yellow). Conductances were calculated from linear fits to steady state I-V data between −60 and −20 mV; average values are from five or more oocytes. The COOH terminus lies between residues 622 and 634.

622) and when that construct is coexpressed with the appropriate complementary segment, suggesting that the COOH terminus of NBD1 lies between aa's 622 and 634. (In other words, it could lie at aa 623, or 624, or 625, etc., but could extend as far as aa 633.) An alternative possibility, that a crucial part of NBD1 extends beyond aa 633 but can nevertheless associate with the Flag3-633 segment to form a complete NBD1 domain, is rendered unlikely by our finding that strong CFTR channel activity was reconstituted by coexpression of Flag3-633 with 668-1480: despite this omission of the 34-residue segment aa's 634–667, basal and activated conductances (16 ± 1 and 175 ± 7 μS, respectively; Fig. 2 and Table I) were similar to those of WT CFTR. On the other hand, oocytes coexpressing Flag3-622 plus 634-1480, in which any CFTR channels must lack aa's 623–633, displayed negligible basal and activated conductances like those of uninjected oocytes.

Defining the NH_2-terminal Boundary of NBD1

We used a similar strategy to incrementally extend the NH_2 terminus of segment 590-1480 in an attempt to build a complete NBD1 there. Upon coexpression with Flag3-589, the extended segment 449-1480 yielded conductances indistinguishable from those of uninjected oocytes, but extended segment 433-1480 gave substantial activated (129 ± 12 μS) conductance, though still smaller than that of WT CFTR-injected oocytes (Fig. 3). However, omission of the overlapping section (residues 433–589) by coexpression of Flag3-432 plus 433-1480 resulted in somewhat larger basal (6 ± 1 μS) and activated (157 ± 5 μS) conductances that approached those of oocytes expressing WT CFTR channels. The fact that coexpression of Flag3-432 plus 449-1480 yielded no functional channels confirms that segment 433-448 is an essential part of NBD1. In contrast, coexpression of Flag3-414 plus 433-1480, which effectively deleted the 18-residue segment aa's 415–432, nevertheless resulted in oocytes that displayed basal and activated conductances (7 ± 1 and 195 ± 5 μS, respectively) comparable with those of oocytes expressing intact CFTR (Fig. 2 and Table I). These data suggest that the NH_2-terminal boundary of NBD1 lies between aa's 432 and 449.

As a control test, each individual segment of CFTR used to investigate the functional boundaries of NBD1 was expressed by itself in oocytes, and basal and activated conductances were measured in the usual manner. In all cases, the resulting conductances were similar to those of uninjected oocytes (Fig. 4), confirming that none of these truncated CFTR fragments readily forms viable channels when expressed alone in *Xenopus* oocytes.

Expression and Maturation of Severed CFTR Segments

Western blots of proteins resolved from whole oocyte membrane preparations were used to evaluate expression of intact or truncated CFTR proteins. As expected, the R-domain antibody did not recognize the Flag3-622 or Flag3-633 segments (Fig. 5 A, lanes 1 and 2), but did detect a single sharp band of ~95 kD (Fig. 5 A, lane 3, thin arrow) when segment 634-1480 was expressed alone. However, an additional broad band of ~150 kD appeared when 634-1480 was coexpressed with Flag3-633

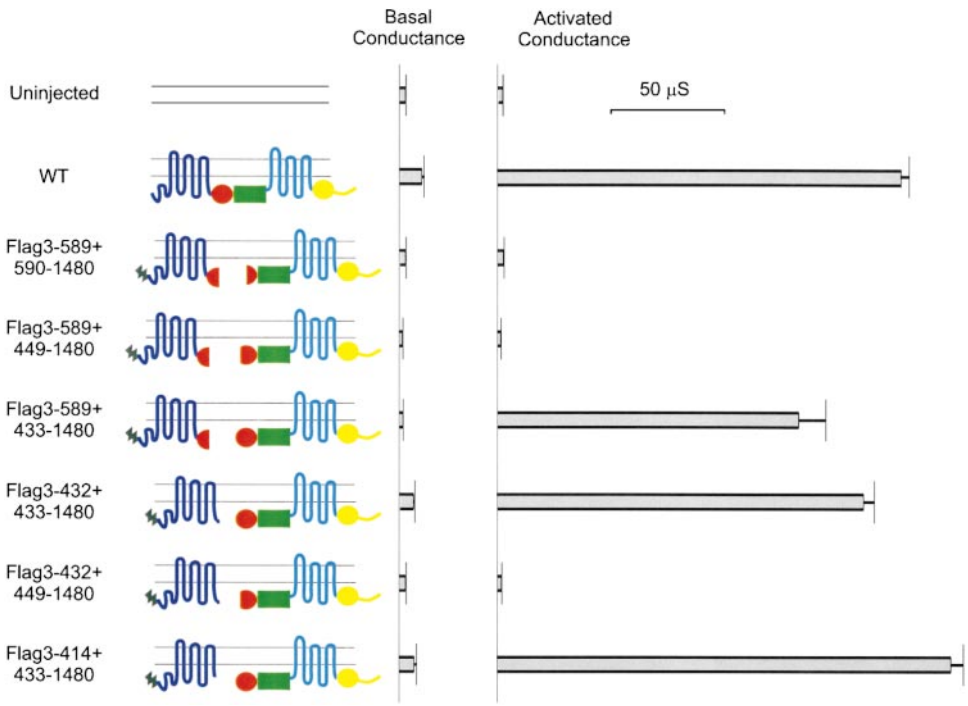

Figure 3. Defining the NH_2-terminal boundary of NBD1 by coexpressing severed CFTR channel segments. Methods and symbols are as in Fig. 2. The NH_2 terminus was found to lie between residues 432 and 449.

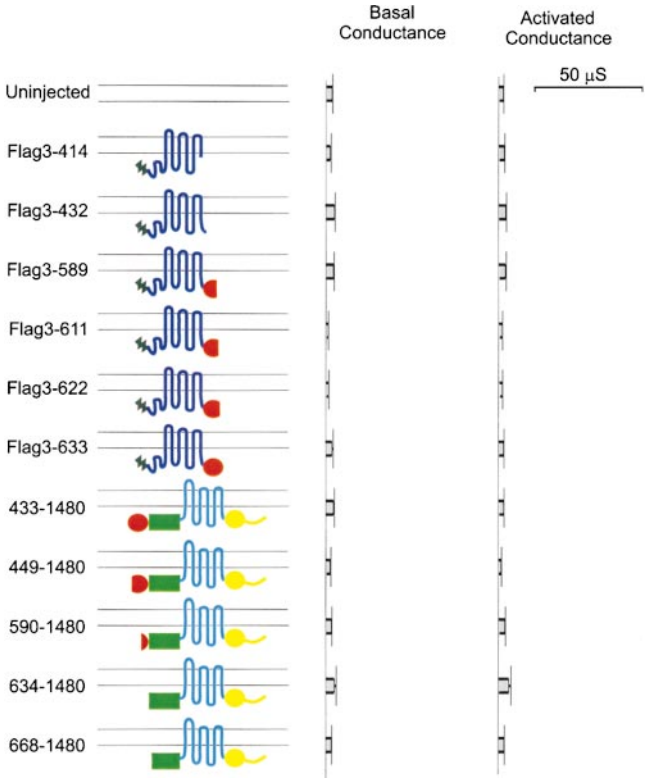

Figure 4. Negligible basal and activated conductances of oocytes injected with 2.5 ng cRNA encoding the indicated single truncated CFTR channel segments. Methods and symbols are as in Fig. 2.

(Fig. 5 A, lane 5, fat arrow), implying that segment 634-1480 was then glycosylated. Accordingly, the ~95-kD band could be digested to a perceptibly smaller band of ~90 kD (Fig. 5 C, thin arrows) by either endoglycosidase-H or *N*-glycosidase-F, whereas the broad ~150-kD (Fig. 5 C, fat arrow) band was insensitive to endoglycosidase-H, but was largely digested to a ~90-kD band after treatment with *N*-glycosidase-F (Fig. 5 C). Because endoglycosidase-H may be expected to remove glycosyl moieties only from proteins not yet modified by the early Golgi enzyme mannosidase II, whereas *N*-glycosidase-F removes all asparagine-linked glycosyl groups, these results argue that the ~90-kD band corresponds to the deglycosylated form of segment 634-1480, while the ~95- and ~150-kD bands correspond to its core glycosylated and fully glycosylated forms, respectively. This, in turn, suggests that segment 634-1480 was merely core glycosylated when expressed alone (Fig. 5 A, lane 3), but could be fully glycosylated when it was coexpressed with the contiguous segment Flag3-633 (Fig. 5 A, lane 5). Together with the several-fold increase in density of the 634-1480 signal in the presence of Flag3-633 (compare lanes 3 and 5), these findings indicate that maturation and stabilization of segment 634-1480 are promoted by its coexpression with an appropriate complementary segment such as Flag3-633. Interestingly, however, the ~150-kD band was not detected when segment 634-1480 was coexpressed with Flag3-622 (Fig. 5 A, lane 4). This, despite the fact that the Flag3-633 and Flag3-622 segments, detected by the anti–Flag M2 antibody as single narrow bands (Fig. 5 B), were both expressed at similar levels, and at almost the same level whether expressed alone or

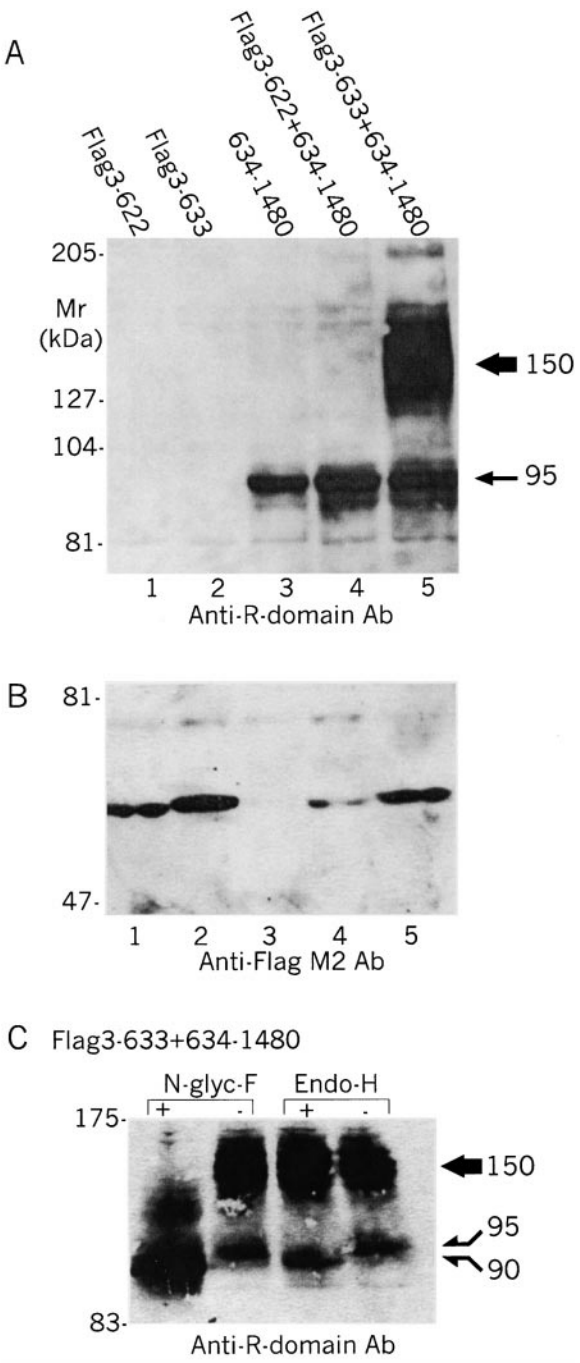

Figure 5. Protein expression of CFTR constructs severed near the COOH terminus of NBD1. (A and B) Immunoblots of membrane proteins from oocytes expressing individual CFTR segments or pairs of segments, as indicated, resolved by SDS-PAGE, transferred, and blotted with anti–R-domain antibody (A) or with anti–Flag M2 antibody (B). (C) Coexpressed constructs Flag3-633 plus 634-1480 were digested with *N*-glycosidase-F (left) or endoglycosidase-H (right), and the products were identified with anti–R-domain antibody. Arrows in A and C mark fully glycosylated (~150 kD, fat arrow), core glycosylated (~95 kD, thin arrow), and deglycosylated (~90 kD, thin arrow) forms of the 634-1480 protein.

coexpressed with 634-1480. Thus, although removal of the eleven residues (aa's 623–633) from Flag3-633 did not affect the stability of the resulting segment, Flag3-622 (Fig. 5 B, lanes 2 and 5 vs. 1 and 4), this deletion abrogated the ability of that segment to promote glycosylation of the coexpressed fragment, 634-1480 (Fig. 5 A, lane 5 vs. 4). These data indicate that completion of the COOH terminus of segment Flag3-622 by some or all of aa's 623–633 is required for productive interaction with segment 634-1480, which, in turn, seems essential for maturation of the resulting complex. This is consistent with the conclusion from the functional measurements, using two-electrode voltage clamp, that the COOH terminus of NBD1 lies between residues 622 and 634.

Similarly, the R-domain antibody did not detect the Flag3-432 segment (which lacks an R domain; Fig. 6 A, lane 1), but recognized segment 433-1480, which, when expressed alone, gave a sharp band at ~125 kD (Fig. 6 A, lane 2, thin arrow). Coexpression of 433-1480 with Flag3-432 (Fig. 6 A, lane 5) yielded that same band (thin arrow), together with an additional, broader band (fat arrow) of ~160 kD (together with weak degradation bands ~70–75 kD), consistent with glycosylation of segment 433-1480. Indeed, after treatment with either endoglycosidase-H or *N*-glycosidase-F the lower (~125-kD) Mr band migrated as a slightly smaller fragment of ~120 kD (Fig. 6 B, thin arrows). On the other hand, the higher (~160-kD; Fig. 6 B, fat arrow) Mr band was insensitive to endoglycosidase-H, but was converted to a ~120-kD band by *N*-glycosidase-F. It seems, then, that the ~120-kD band represents the unglycosylated form of segment 433-1480, while the ~125- and the ~160-kD bands represent its core glycosylated and fully glycosylated forms. However, hardly any protein was detected (over the range ~45 to ~180 kD) by the R-domain antibody when segment 449-1480 was expressed alone (Fig. 6 A, lane 3). Even when it was coexpressed with the Flag3-432 segment, only a relatively weak band of ~70 kD could be detected, presumably representing a degraded form of 449-1480 protein (Fig. 6 A, lane 4, *). So, it appears that the stability of 449-1480 protein was slightly increased in the presence of Flag3-432, although no glycosylated form of 449-1480 was observed. Thus, deletion of aa's 433–448 from 433-1480 yielded a segment that seemed highly unstable, even when coexpressed with a complementary segment of CFTR. These biochemical findings support our conclusion from the electrophysiological assays of function that the NH_2 terminus of NBD1 lies between residues 432 and 449.

Physical Association between Complementary Fragments Starts in the Endoplasmic Reticulum

Coimmunoprecipitation tests were made using anti–Flag M2 affinity beads to evaluate physical association between Flag-tagged NH_2-terminal segments of CFTR

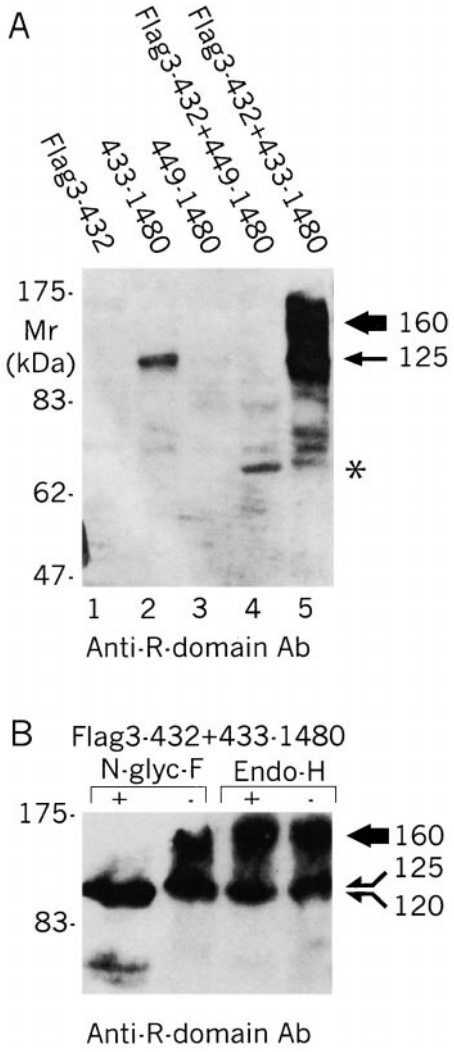

Figure 6. Protein expression of CFTR constructs severed near the NH_2 terminus of NBD1. (A) Immunoblot of membrane proteins from oocytes expressing individual CFTR segments or pairs of segments, as indicated, blotted with anti–R-domain antibody. (B) Coexpressed constructs Flag3-432+433-1480 were digested with *N*-glycosidase-F (left) and endoglycosidase-H (right), and the products were identified with anti–R-domain antibody. Arrows in A and B mark fully glycosylated (~160 kD, fat arrow), core glycosylated (~125 kD, thin arrow), and deglycosylated (~120 kD, thin arrow) forms of 433-1480 protein. *Partially degraded form (~70 kD).

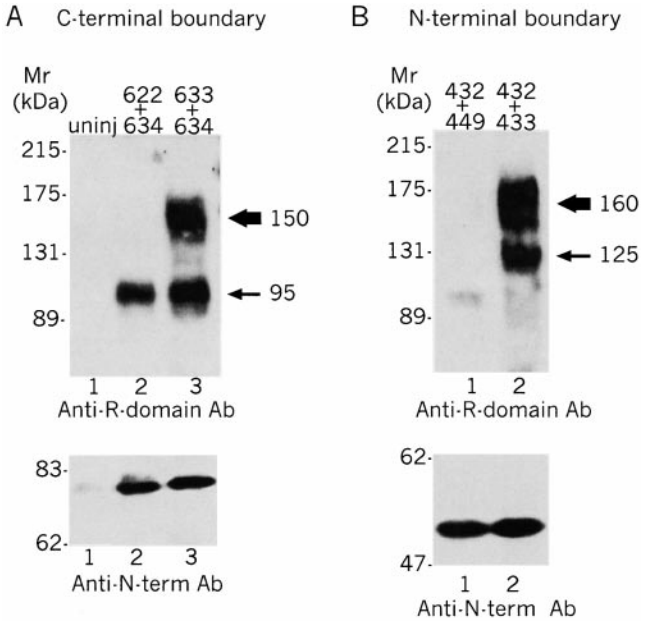

Figure 7. Coimmunoprecipitation of severed CFTR constructs. Digitonin-solubilized membrane proteins were immunoprecipitated with anti–Flag M2 affinity beads, eluted, resolved with SDS-PAGE on 7.5–10% gradient gels, and blotted with anti–R-domain antibody (top) or anti–NH_2-terminus antibody (bottom). (A) Constructs severed near the COOH terminus of NBD1: uninjected (lane 1), Flag3-622+634-1480 (lane 2), Flag3-633+634-1480 (lane 3); arrows are as in Fig. 5 A. (B) Constructs severed near the NH_2-terminus of NBD1: Flag3-432+449-1480 (lane 1), Flag3-432+433-1480 (lane 2); arrows are as in Fig. 6 A.

and complementary COOH-terminal segments in membrane extracts from oocytes coinjected with cRNAs encoding severed CFTR molecules. Both segments Flag3-622 and Flag3-633 (detected with an antibody against an epitope near CFTR's NH_2 terminus; Fig. 7 A, bottom, lanes 2 and 3) were able to coimmunoprecipitate the core glycosylated (~95-kD; thin arrow) form of segment 634-1480 (top, lanes 2 and 3). However, the fully glycosylated (~150-kD; fat arrow) form of 634-1480 was coimmunoprecipitated only with Flag3-633 (Fig. 7 A, top, lane 3) and not with Flag3-622 (lane 2). Because the immunoprecipitation was via the Flag tag, it appears that both Flag3-622 and Flag3-633 segments associate with the core glycosylated segment 634-1480 (Fig. 7 A, top, lanes 2 and 3, thin arrow), presumably in the endoplasmic reticulum (ER), but only the Flag3-633 plus 634-1480 complex proceeds to the Golgi compartment, and eventually to the cell surface membrane as a mature, fully glycosylated channel. The Flag3-622 plus 634-1480 complex (Fig. 7 A, lane 2), on the other hand, does not appear to leave the ER.

Correspondingly, immunoprecipitation of segment Flag3-432 (detected with the anti–NH_2-terminal antibody; Fig. 7 B, bottom, lanes 1 and 2) resulted in coimmunoprecipitation of both core-glycosylated (thin arrow) and fully glycosylated (fat arrow) forms of segment 433-1480 (top, lane 2), but of little or no protein corresponding to segment 449-1480 (top, lane 1). The latter result corroborates the conclusion from the Western blot of Fig. 6 A that segment 449-1480 appears to be rapidly degraded in the oocyte. Coimmunoprecipitation (using the anti–Flag beads) of both immature and mature forms of 433-1480 (Fig. 7 B, top, lane 2, thin and fat arrows), however, demonstrates that segments Flag3-432 and 433-1480 physically associate with each

other, and that this association takes place in the ER (or, at the latest, in the early Golgi compartment). These data indicate that the complementary pairs of CFTR segments that constitute functional channels, whether severed just before or just after the intact NBD1, begin their association in the ER before proceeding through the Golgi to the cell membrane, whereas segment pairs that do not comprise an intact NBD1 fail to exit the ER.

The NH_2-terminal Flag Epitope Lowers the P_o of CFTR Channels by Slowing Opening

Forskolin activates CFTR channels indirectly via a pathway that involves adenylyl cyclase and PKA holoenzyme, and, in the oocyte, such activation appears to be subject to saturation (Csanády, L., K.W. Chan, D. Seto-Young, D.C. Kopsco, A.C. Nairn, and D.C. Gadsby, manuscript submitted for publication). Moreover, IBMX at millimolar concentrations likely directly stimulates CFTR channel activity (Al-Nakkash and Hwang, 1999). Both of these facts make our two-microelectrode recordings only coarse assays of the function of CFTR channels, whether intact or severed, expressed in oocytes. We therefore directly activated the channels by applying catalytic subunit of PKA to the cytoplasmic surface of inside-out patches excised from the oocytes, and evaluated their behavior in detail. Also, because the NH_2-terminal CFTR segments described so far had all been tagged with the Flag M2 epitope, we characterized the unitary currents of the three representative channel types, WT CFTR, CFTR severed just before NBD1, and CFTR severed just after NBD1, in each case with and without the Flag tag (e.g., Fig. 8). The representative recordings in Fig. 8 show that WT and Flag-WT CFTR channels share several of the accepted hallmark characteristics, such as single-channel conductance, the requirement for ATP and prior phosphorylation by PKA for channel activity, relatively slow channel gating (interburst and burst durations on the order of seconds), and locking of the channels in the open state by PP_i or by AMPPNP (data not shown). However, kinetic analysis revealed that the P_o of Flag-WT was ~1/3 that of WT (Fig. 9 and Table II). This reduction in P_o was not due to any change in mean burst duration (i.e., in closing rate), but rather reflected an approximately threefold prolongation of the mean interburst duration (i.e., approximately threefold lower opening rate) of Flag-WT compared with WT channels (Fig. 9). Comparable results were obtained when the severed CFTR channels Flag3-432 plus 433-1480 and Flag3-633 plus 634-1480 were compared with their Flag-less counterparts (Fig. 9). As evident from the recordings in Fig. 8, all of these constructs displayed the same general channel characteristics as listed above for WT CFTR channels. Despite this broad similarity, both of the severed CFTR channels containing the NH_2-terminal Flag showed interburst durations two- to threefold longer than those of the corresponding Flag-less severed CFTR channels (Fig. 9 and Table II). Therefore, the Flag epitope added to the NH_2 terminus of CFTR significantly reduces channel P_o by selectively slowing channel opening.

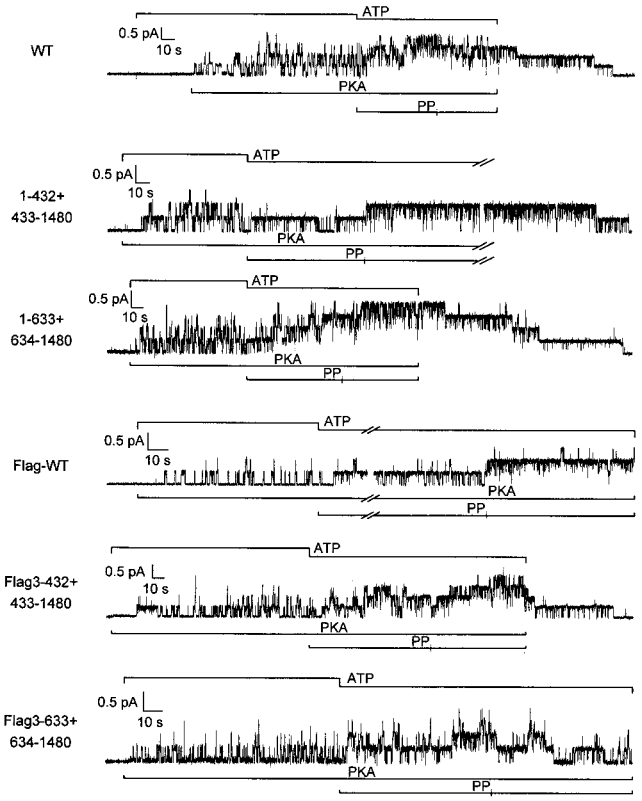

Figure 8. Representative excised-patch current recordings showing WT, 1-432+433-1480, 1-633+634-1480, Flag-WT, Flag3-432+433-1480, and Flag3-633+634-1480 CFTR channels. All constructs displayed hallmark characteristics of WT CFTR including requirement for phosphorylation by PKA (here 300 nM) and exposure to MgATP (here 1 mM for WT, 2 mM for others) for channel activity, slow burst kinetics, and locking in the open state by a mixture of ATP (0.1 mM) and PP_i (2 mM).

TABLE II

Gating Kinetics of Intact and Severed CFTR Channels

Construct	Burst duration	Interburst duration	P_o	*n*
WT (1-1480)	896 ± 145	1604 ± 253	0.36 ± 0.05	9
1-432+433-1480	910 ± 166	2211 ± 485	0.29 ± 0.03	6
1-633+634-1480	554 ± 21*	2380 ± 703	0.22 ± 0.03*	7
Flag-WT (Flag3-1480)	954 ± 375	5050 ± 1326*	0.12 ± 0.02‡	7
Flag3-432+433-1480	921 ± 447	4279 ± 1078*	0.13 ± 0.02‡	6
Flag3-633+634-1480	505 ± 128§	4526 ± 775‡	0.08 ± 0.01‡	5

Mean (±SEM) P_o and burst and interburst durations (ms) of various CFTR constructs at 2 mM MgATP and 300 nM PKA at ~22°C. Values significantly different from WT: *$P < 0.05$, or ‡$P < 0.01$, §$P < 0.1$. *n*, number of observations.

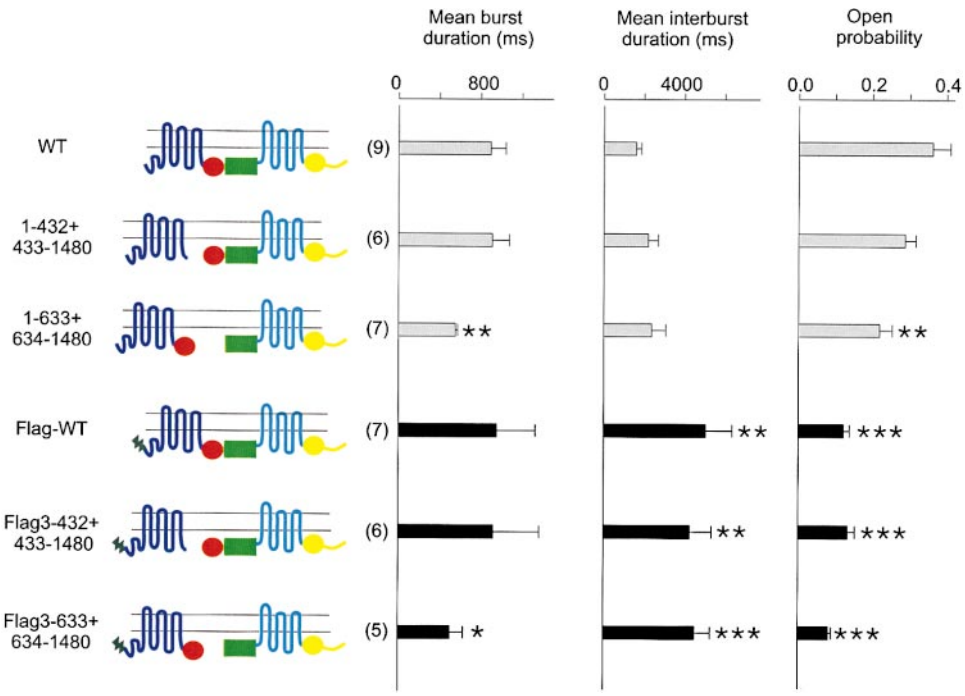

Figure 9. Kinetic analysis of WT, 1-432+433-1480, 1-633+634-1480, Flag-WT, Flag3-432+433-1480, and Flag3-633+634-1480 channels. Kinetic parameters were extracted from records (filtered at 100 Hz, sampled at 1 kHz) of patches containing one to seven channels, exposed to 2 mM MgATP and 300 nM PKA. Mean burst durations of constructs severed between NBD1 and the R domain (1-633+634-1480 and Flag3-633+634-1480) were significantly shorter than those of WT or Flag-WT. All constructs containing the Flag epitope (Flag-WT, Flag3-432+433-1480, and Flag3-633+634-1480) showed significantly prolonged interburst durations and, hence, significantly reduced P_o compared with WT. Significance levels: $*P < 0.1$, $**P < 0.05$, and $***P < 0.01$.

Severing CFTR between NBD1 and the R Domain Lowers P_o by Speeding Channel Closing

The more interesting question is whether severing CFTR, either just before or just after NBD1, affects channel gating. The results of the kinetic analysis (Fig. 9 and Table II) demonstrate that severed channels formed from segments 1-432 plus 433-1480 had a P_o, a mean burst duration, and a mean interburst duration that were not significantly different from those of WT CFTR channels. Furthermore, this similarity was not influenced by addition of the Flag epitope, since severed channels formed from Flag3-432 plus 433-1480 segments showed P_o, and burst and interburst durations, closely similar to those of Flag-WT channels (Fig. 9 and Table II). However, severed channels formed from CFTR segments 1-633 plus 634-1480 had a smaller P_o than WT or 1-432 plus 433-1480 channels, attributable to a reduced burst duration (i.e., to an increased closing rate). This effect of severing CFTR channels just after NBD1 was independent of the presence or absence of the Flag epitope, because the mean burst duration of channels comprising segments Flag3-633 plus 634-1480 was significantly shorter than that of either Flag-WT or Flag3-432 plus 433-1480 channels (Fig. 9 and Table II). These findings indicate that severing CFTR just before NBD1 has no measurable effect on channel P_o or gating kinetics, whereas severing CFTR between NBD1 and the R domain leads to a reduction in P_o due to an increase in channel closing rate.

Neither Adding the Flag Epitope, nor Severing CFTR before or after NBD1, Affects Single-Channel Conductance or the Apparent Affinity for ATP

To verify that neither incorporating the Flag epitope nor severing CFTR before or after NBD1 causes a major structural alteration in the channel pore, we measured single-channel conductances of WT and Flag-WT CFTR channels, and of severed channels formed from segments 1-432 plus 433-1480, or Flag3-432 plus 433-1480, or 1-633 plus 634-1480, or Flag3-633 plus 634-1480, in excised patches exposed to symmetrical 140 mM Cl^- solutions. Under these conditions, as illustrated for WT and for 1-432 plus 433-1480 channels, each channel type was characterized by an ohmic single-channel conductance: its average magnitude was ~7 pS and there was no significant difference between the conductance of WT CFTR channels and that of any of the other constructs ($P = 0.1$; Fig. 10). This argues that severing CFTR, or adding the NH_2-terminal Flag, did not grossly alter the pore architecture.

Assuming that a step after binding of ATP at one of the NBDs rate limits channel opening (see Csanády and Gadsby, 1999; Gadsby and Nairn, 1999; Zeltwanger et al., 1999), there are two possible explanations for the observation that opening rate, and hence P_o, are decreased in Flag-tagged CFTR channels. This decrease could result from a reduction either in the binding affinity for ATP at that site, or in the rate of a step after binding (such as a step related to hydrolysis, or trans-

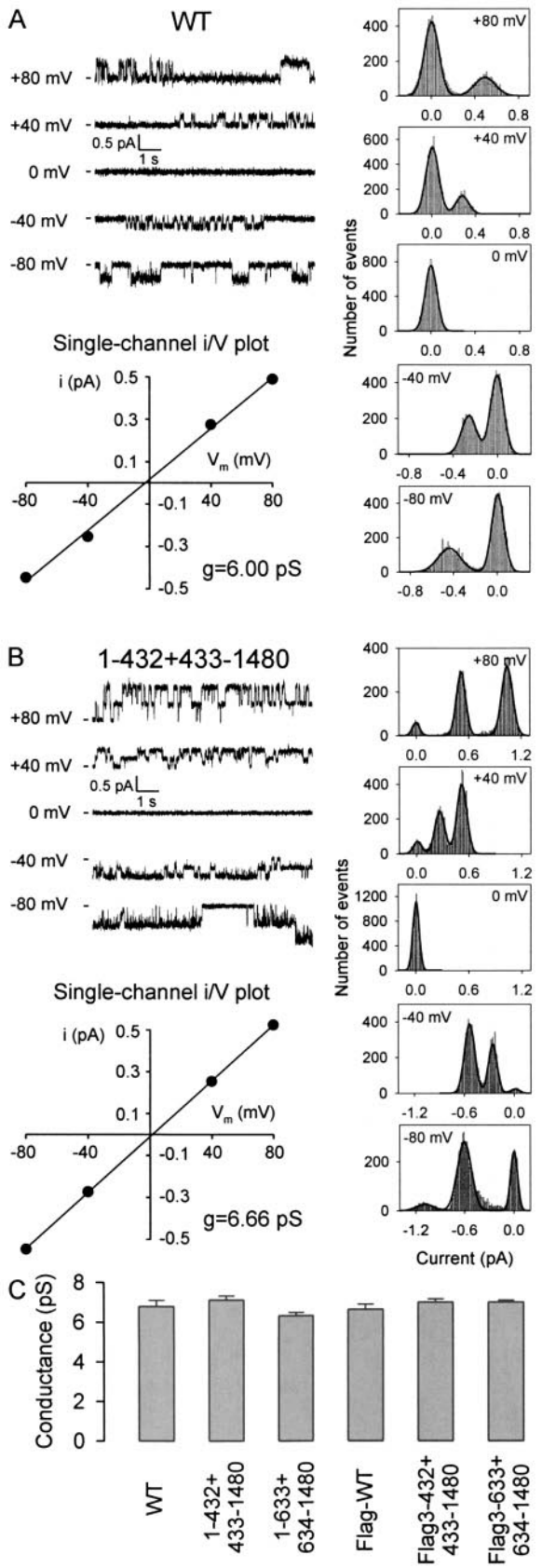

Figure 10. Single-channel conductances of WT, 1-432+433-1480, 1-633+634-1480, FlagWT, Flag3-432+433-1480, and Flag3-633+634-1480 channels in symmetrical 140 mM Cl^-. (A and B) Segments of representative CFTR channel current records, illustrated for WT and 1-432+433-1480, at holding potentials of −80, −40, 0, +40, and +80 mV, were used to create amplitude histograms, fitted by sums of Gaussians (right). The distances between adjacent peaks, plotted against potential gave linear I-V plots. (C) Fitted slopes gave conductances of 6.8 ± 0.3 (WT), 7.1 ± 0.2 (1-432+433-1480), 6.3 ± 0.2 (1-633+634-1480), 6.6 ± 0.3 (Flag-WT), 7.0 ± 0.2 (Flag3-432+433-1480), and 7.0 ± 0.1 (Flag3-633+634-1480), none of which differed significantly from WT at $P < 0.1$.

mission of the gating conformational change to the pore). To distinguish between these two possibilities, for each CFTR construct we measured macroscopic currents in large patches containing many channels, and compared the current magnitude during a test exposure to 50 μM MgATP with that obtained at 2 mM MgATP, just before and after the test (Fig. 11). The ratio of these currents ($I_{50\mu M}/I_{2mM}$) provides a rough measure of apparent affinity for ATP because, for all constructs, 2 mM MgATP proved to be a saturating concentration; thus, I_{1mM}/I_{2mM} ratios were 1.01 ± 0.03 for WT, 0.94 ± 0.03 for 1-432+433-1480, 1.30 ± 0.10 for 1-633+634-1480, 1.02 ± 0.04 for FlagWT, 0.96 ± 0.03 for Flag3-432+433-1480, and 1.15 ± 0.09 for Flag3-633+634-1480. Both the representative macroscopic current records for each of these constructs and the bar graph summary (Fig. 11) show that the $I_{50\mu M}/I_{2mM}$ ratios were all very similar and close to 0.5, indicating that $K_{1/2}$(ATP) for activation of P_o (since the time-averaged number of active channels may be assumed constant during these bracketed measurements) was ~50 μM for all these constructs. Hence, the observed reduction in P_o after addition of the Flag epitope to the NH_2 terminus of CFTR (Fig. 9) is likely to reflect slowing of a rate-limiting step after ATP binding.

Deletion of aa's 415–432 in CFTR Does Not Alter the Apparent Affinity for ATP

The demonstration that effective deletion of aa's 415–432, by coexpression of segments Flag3-414 and 433-1480, impairs CFTR channel activity very little, if at all (Fig. 3), has ramifications for our understanding of the relationship between the structure of these channels and their function. This is because residues 415-432 in CFTR align (Fig. 12, below) with those comprising the first β strand in the recently solved high-resolution structures of HisP, the NBD of histidine permease (from *Salmonella typhimurium*; Hung et al., 1998), and of the NH_2-terminal NBD in RbsA, which incorporates the two NBDs of the ribose transporter (from *Escherichia coli*; Armstrong et al., 1998). Although the sequences of these three NBDs (NBD1 of CFTR, NH_2-terminal NBD of RbsA, and HisP) share only on the order of 20% identity, largely restricted to the highly conserved ABC signature sequence and to the Walker A and B sequences (Walker et al.,

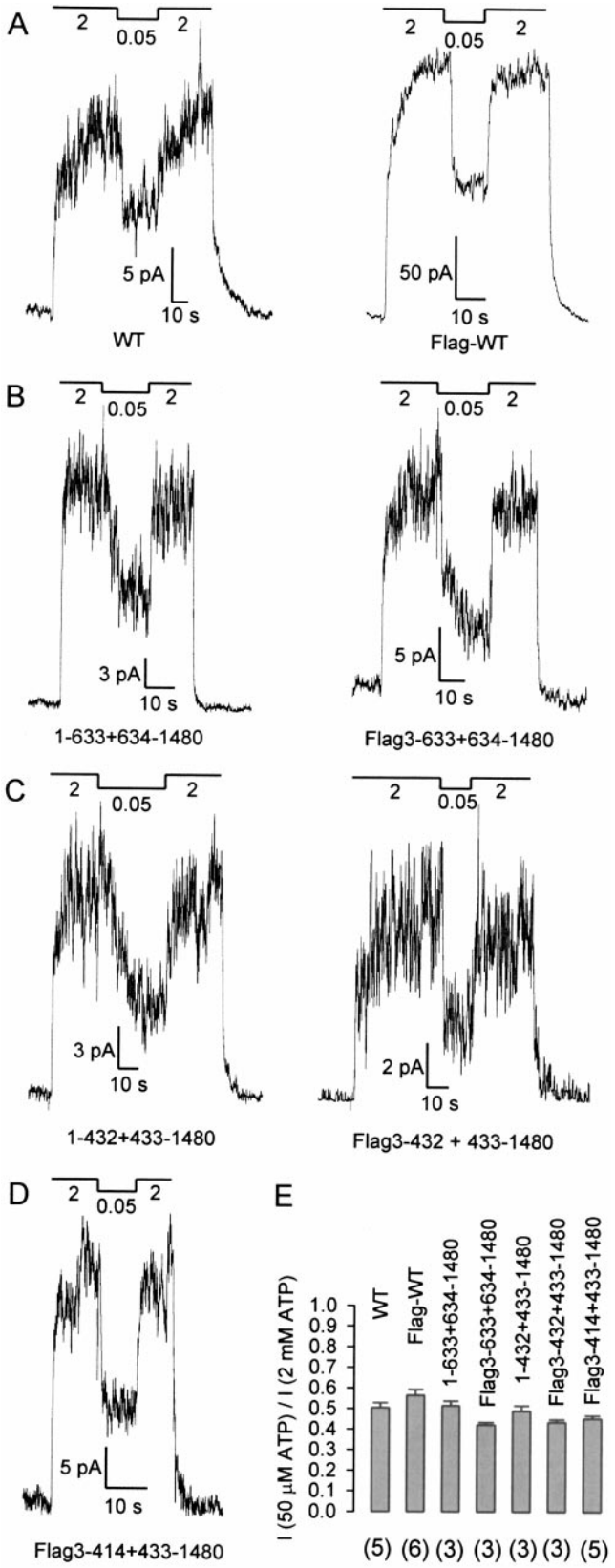

Figure 11. Apparent affinities for activation of channel P_o by MgATP. Representative macropatch currents are shown for WT and Flag-WT (A), 1-633+634-1480 and Flag3-633+634-1480 (B), 1-432+433-1480 and Flag3-432+433-1480 (C), and Flag3-414+433-1480 (D) channels. After prephosphorylation by PKA, and removal of both PKA and ATP, once all channels had closed, 50 μM ATP was applied for 10–30 s, bracketed between exposures to 2 mM ATP. (E) The ratios of the mean steady currents, $I_{50\mu M}/I_{2mM}$, were 0.50 ± 0.02 (WT), 0.56 ± 0.03 (Flag-WT), 0.51 ± 0.02 (1-633+634-1480), 0.42 ± 0.01 (Flag3-633+634-1480), 0.49 ± 0.02 (1-432+433-1480), 0.44 ± 0.01 (Flag3-432+433-1480), and 0.45 ± 0.01 (Flag3-414+433-1480). None of the constructs differed significantly from WT at $P < 0.05$.

1982), because the latter both contribute to the active site, and yet are separated by ~140 residues in HisP, this large distance strongly constrains alignments of different NBD sequences (Hung et al., 1998). Moreover, despite the small degree of identity, the catalytic site architectures of HisP and RbsA are closely similar: both resemble an open cup, formed by a broken β-barrel, within which the nucleotide binds (Hung et al., 1998). In both crystal structures, a conserved aromatic residue, Tyr16 in HisP and Phe14 in RbsA, located at the end of the first β strand (Fig. 12, below), makes extensive hydrophobic contact with the adenine base of the bound nucleotide and, at least in HisP, seems crucial for nucleotide binding (Shyamala et al., 1991; Hung et al., 1998). Depending on the alignment, the corresponding residue in NBD1 of CFTR is likely to be Leu435 (Fig. 12, below; compare Hung et al., 1998), or perhaps Phe433. Insofar as the structure of NBD1 in CFTR resembles those of HisP and RbsA, the deletion of aa's 415–432 may be expected to remove the entire first β strand, which, in turn, through its proximity to Phe433 and Leu435, would be anticipated to influence nucleotide binding. To see whether this deletion affects the apparent affinity for ATP activation of channel P_o, we measured the ratio $I_{50\mu M}/I_{2mM}$ for Flag3-414+433-1480 CFTR channels in macropatches (Fig. 11). This ratio was found to be close to 0.5 for Flag3-414+433-1480 channels, the same value as observed for WT (as well as all the other CFTR constructs tested in Fig. 11). Since, in one experiment, I_{1mM}/I_{2mM} was 1.02 in a macropatch of Flag3-414+433-1480 channels, we may conclude that $K_{1/2}$ (ATP) was ~50 μM for these channels also.

DISCUSSION

In this work, we have demonstrated that physical and functional association of complementary segments of CFTR, severed just before or after NBD1, results in split channels with microscopic properties closely similar to those of intact WT CFTR. Further, by systematically shifting the sever point, we have been able to define the domain boundaries of NBD1 to within 10–15 amino acids. The newly defined boundaries have important ramifications for structural and functional studies of CFTR's NBDs, whether as isolated polypeptides or in their native state, incorporated into full-length CFTR.

That a severed membrane transport protein may nevertheless function has been demonstrated previously. For example, *E. coli* cells expressing both putative hexahelical halves of *lac* permease, severed within its central cytoplasmic loop, transport lactose at about one third the rate of cells expressing intact permease, but no transport is seen in cells expressing either half alone (Bibi and Kaback, 1990). Similarly, coexpression in *Xenopus* oocytes of up to three complementary segments (severed within cytoplasmic or extracellular loops) comprising the full-length human erythrocyte anion exchanger (band 3, or AE1) resulted in Cl^- influx levels comparable with those observed after expression of intact WT band 3 (Groves et al., 1998). Although the domain organization of band 3 is not yet known, it is remarkable that the protein backbone can be cut at at least four sever points (and at at least two of them simultaneously) with little detectable loss of Cl^- transport function. It is perhaps less surprising that a known multidomain protein like the voltage-gated Na channel, which has four repeats, each with six putative membrane-spanning helices, can still function with a single cut between two repeats (at least, in two of the three linking loops; Stühmer et al., 1989). Eukaryotic ABC transporters are also multidomain proteins with homologous internal repeats, a consequence of their evolution from prokaryotic ancestors in which the individual domains are often expressed from separate genes (e.g., Higgins, 1992). So it is not surprising that ABC molecules such as the yeast **a**-factor transporter, STE6, can also function when coexpressed as two separate halves (Berkower and Michaelis, 1991), nor that coimmunoprecipitation experiments demonstrate that those two halves physically interact (Berkower et al., 1996). Representatives of the two families of multidrug-resistance ABC proteins, Pgp (Loo and Clarke, 1994) and MRP (Gao et al., 1996) have also been shown to survive being cut in half, between NBD1 and the second transmembrane domain, and to retain at least partial function: severed MRP transported substrate at least a third as well as intact MRP (a fraction possibly simply reflecting the efficiency of simultaneous transfection of the insect cells used; Gao et al., 1996), whereas severed Pgp supported substrate-induced ATPase activity about half that of intact Pgp, but showed no sign of drug transport in NIH-3T3 cells, possibly due to defective trafficking to the cell membrane (Loo and Clarke, 1994). Physical and functional association between NH_2- and COOH-terminal halves of CFTR (residues 1-835 and 837-1480; cut after the R domain) was demonstrated by Ostedgaard et al. (1997), who found that the severed construct supported intracellular cAMP-activated anion fluxes, assayed by measurements of SPQ fluorescence, that were comparable with those of WT CFTR.

Assaying the function of severed molecules to define domain boundaries is an approach well suited to multidomain, single-gene eukaryotic ABC transporters, because individual domains may each correspond to the product of a single ancestral gene and may therefore reasonably be expected to be capable of folding separately. Indeed, there are already several examples of putative links between domains of such eukaryotic ABC proteins being severed without destroying the molecule's overall function (as described above). In general, if severing the backbone of a protein does not detectably impair its function, it is reasonable to conclude that covalent linkage at that point is not required for the assayed function. It may further be concluded either that the cut occurs between functional domains, or that the sever point lies within such a domain but the native fold and function are nevertheless retained (Shiba and Schimmel, 1992; Betton and Hofnung, 1994). However, the latter possibility becomes far less likely if function remains intact when a substantial deletion is introduced on one side or the other of the sever point. That was precisely our finding when we effectively deleted the 18-residue segment 415-432 (by coexpressing Flag3-414 plus 433-1480; Fig. 3) from the NH_2-proximal side of NBD1, or the 34-residue segment 634-667 (by coexpressing Flag3-633 plus 668-1480; Fig. 2) from the COOH-proximal side of NBD1 (Fig. 12, gray). In contrast, we could detect neither function nor mature protein when we simply introduced a single cut (Fig. 12, red) only 16 or 11 residues away from those deletions, respectively, but in the direction of the conserved core of the domain. Therefore, the domain boundaries of NBD1 of CFTR, as defined by the assays of microscopic function used here, can be confidently assigned to lie within residues 433–448 and 623–633 at the NH_2 and COOH termini of NBD1, respectively.

In the present work, we have made detailed single-channel measurements that show that individual severed CFTR channels, cut just before (1-432 plus 433-1480) or after (1-633 plus 634-1480) NBD1, have the same unitary conductance as WT CFTR channels (Fig. 10) and almost identical microscopic gating characteristics in the presence of PKA catalytic subunit (Fig. 9). Both severed constructs had the same opening rate as WT channels, and the same apparent affinity for activation of channel P_o by MgATP, and both were locked open by PP_i (Fig. 8) or AMPPNP. Only the closing rate of channels cut after NBD1 differed from that of WT, and was ~40% faster, indicating that the bursting state is somewhat destabilized by that cut, due to a slight acceleration of the rate-limiting step for channel closing (likely reflecting speeding of the slowest step in the ATP hydrolysis cycle at NBD2; Csanády et al., 2000). Thus, we can conclude that the normal gating function of NBD1 (which we and others infer to be control of channel opening; for reviews, see, e.g., Csanády and Gadsby, 1999; Gadsby and Nairn, 1999) does not de-

Figure 12. Alignment of CFTR's NBD1 with HisP. PSI-Blast aligned CFTR residues 422–637 with corresponding residues in HisP. Secondary structure elements shown below (β-strands, magenta arrows; α-helices, orange boxes) correspond to those of the solved crystal structure of HisP (Hung et al., 1998). CFTR residue numbers are centered above the corresponding letters. Teal boxes identify the three consensus sequences conserved in most ABC proteins. Red boxes in the CFTR sequence identify nontolerated, green boxes tolerated, cut sites. (Cuts occurred between the two highlighted residues in each case.) Gray boxes identify sections flanking the NBD1 sequence that could be omitted without destroying channel function. *Residue F508.

pend on its covalent linkage either to the first transmembrane domain or to the R domain, since the maximal opening rates are the same for intact channels as for channels cut before or after NBD1 (Fig. 9). Nor does channel opening require segments 415-432 (Figs. 3 and 11) or 634-667 (Fig. 2). On the other hand, we found a consistent and significant effect of incorporating the eight-residue Flag tag at the NH_2 terminus of CFTR, which reproducibly slowed channel opening approximately two- to threefold, resulting in an approximately two- to threefold reduction in P_o for both severed and intact constructs, without affecting the mean burst duration, conductance, or locking of any of the channels. It is notable that attaching the 238-residue green fluorescent protein (GFP) to the NH_2 terminus of CFTR was found to affect neither single-channel conductance (assayed in bilayers) nor macroscopic whole-cell conductance in transfected NIH-3T3 cells (Moyer et al., 1998). But it remains unclear whether channel P_o was affected by the large GFP tag, because the bilayer experiments did not address channel number or gating kinetics, and no comparison was made between the levels of CFTR protein expressed in cells transfected with WT CFTR and those transfected with GFP-CFTR. Interestingly, an interaction between an acidic region of CFTR's NH_2-terminal cytoplasmic tail and the R domain was recently demonstrated, which stabilized the open state of the channel (Naren et al., 1999); disrupting the interaction by mutating the acidic residues resulted in shorter bursts. It is not yet clear whether, or how, that finding relates to our observation here that incorporation of the largely acidic Flag at the NH_2 terminus of CFTR stabilized the channel closed state (both for intact and severed channels). We have found, however, that this effect is also mediated via the R domain, since addition of an NH_2-terminal Flag does not alter the opening rate of severed CFTR channels from which the entire R domain (aa's 634–836) is missing (Csanády, L., K.W. Chan, D. Seto-Young, D.C. Kopsco, A.C. Nairn, and D.C. Gadsby, manuscript submitted for publication).

None of the half-molecule constructs gave measurable basal or activated Cl^- conductance in two-microelectrode recordings of macroscopic currents, regardless of whether the oocytes were expressing the NH_2-terminal half with (construct Flag3-835; not illustrated) or without (Flag3-633; Fig. 4) the R domain, or the COOH-terminal half with (CFTR construct 634-1480; Fig. 4) or without (construct 837-1480; not illustrated) the R domain. However, because we did not record from patches excised from those oocytes, we cannot rule out the possibility that an extremely low density of channels might be formed from certain half molecules. Our macroscopic current results contrast with a recent report that expression of only the COOH-terminal half of CFTR, either with or without the R domain, gave macroscopic, intracellular cAMP-activated, whole-cell currents in injected oocytes and in transfected IB3 cells, as well as unitary currents activated by PKA and ATP in patches excised from the IB3 cells (Devidas et al., 1998). Although a major procedural difference was the injection of 50 ng cRNA per construct in those experiments (vs. 2.5 ng in ours), it seems unlikely that protein expression was correspondingly high because the activated conductance of WT CFTR was only ≤10 μS (Devidas et al., 1998), more than 20-fold smaller than the average in the present experiments (Figs. 1–3, Table I). Sheppard et al. (1994) did observe channel currents in

patches excised from HeLa cells expressing just the NH_2-terminal half of CFTR truncated after the R domain (segment 1-835), though channel formation was far less efficient than for WT CFTR, which presumably accounts for the fact that no change in SPQ fluorescence could be detected when the same cells were challenged with cAMP-elevating cocktail (Ostedgaard et al., 1997).

How do the boundaries of CFTR's NBD1 that we have functionally defined here compare with the crystal structures of the HisP and RbsA NBDs, whose close similarity to each other supports their being considered reasonable models for the structure of all ABC NBDs, including those of CFTR? Although the safe boundaries of CFTR's NBD1 (433-633) circumscribe only 200 residues, whereas the crystallized NBDs of HisP and RbsA included 259 and 241 residues, respectively, they still compare reasonably well because alignments (e.g., Fig. 12; compare Hung et al., 1998) indicate that NBD1 of CFTR lacks a stretch of 20–30 amino acids present in the other NBDs. Moreover, the safe sever points can be rationalized on the basis of such alignments. Thus, Phe433 would be predicted to occur near the end of the first β strand (Fig. 12), some distance from the γ-phosphate of bound ATP (although nearby Leu435, if not Phe433 itself, is implicated in binding of the nucleotide base; see Hung et al., 1998), and Leu633 would be expected to occur after the final β strand in the NBD structure, between it and a pair of final helices (arranged slightly differently in HisP and RbsA). In contrast, the nontolerated sever point Glu449 occurs just before a highly conserved glycine that in HisP and RbsA begins a β strand at the center of the β sheet that forms the major wall of the active site, where severing might be anticipated to disrupt its structure. At the COOH terminus, Gly622 is predicted to lie in the loop connecting the last two (antiparallel) β strands of that large β sheet, where severing might perturb stabilizing interactions between those two strands. Overall, that the structures of HisP and RbsA afford reasonable interpretations of our results with NBD1 of CFTR supports the notion that the NBDs of all ABC transporters are likely to share the same general fold. If so, our findings have importance for the design of peptide models of CFTR's NBDs and imply, for instance, that CFTR NBD1 constructs truncated at or near residue 589 would be structurally incomplete and hence functionally disadvantaged (see Hartman et al., 1992; Ko and Pedersen, 1995; Ko et al., 1997; Clancy et al., 1998), as might CFTR NBD2 constructs truncated at Leu1399 (corresponding to NBD1 Leu602; Randak et al., 1996, 1997).

The finding that severed CFTR channels lacking residues 415-432 (i.e., coexpressed Flag3-414 plus 433-1480) are opened by MgATP with the same apparent affinity as seen for WT CFTR channels ($K_{1/2} \sim 50$ μM; Fig. 11) is intriguing. This is because a number of observations have suggested that it is binding of ATP at NBD1 (and possibly hydrolysis of that ATP) that is responsible for CFTR channel opening (reviewed in Csanády and Gadsby, 1999; Gadsby and Nairn, 1999). For example, CFTR 1-835 channels, truncated after the R domain and hence lacking NBD2, are opened by MgATP with micromolar apparent affinity (Sheppard et al., 1994), and CFTR 1-1218 channels, also lacking NBD2, yield large currents in whole oocytes and robust channel gating in excised patches (Chan et al., 1999). Moreover, mutant K1250A CFTR channels, in which ATP hydrolysis at NBD2 is severely impaired (Ramjeesingh et al., 1999), show brief WT-like openings at low micromolar [ATP], but extremely long openings at higher [ATP] that reflect binding at NBD2 of ATP that cannot be hydrolyzed (Zeltwanger et al., 1999); those results imply that the brief openings at low [ATP] involve only NBD1. It is, nevertheless, possible that the binding site responsible for channel opening is not formed entirely by NBD1. If the relatively high affinity action of MgATP to open CFTR channels does indeed occur at NBD1 even in Flag3-414 plus 433-1480 channels, then our findings prompt a new series of questions. Thus, despite an overall similarity in the organization of the NBDs of all ABC transporters, perhaps the detailed structure of the nucleotide binding pocket of NBD1 in CFTR differs from that of HisP or RbsA? Or, perhaps the detailed structures are similar, but our expectations of the consequences of deleting the β strand formed by residues 415-432 are unwarranted? Alternatively, perhaps substantial contributions to the binding energy for MgATP at NBD1 are made by other regions of the CFTR polypeptide, such as NBD2 (e.g., Jones and George, 1999) or cytoplasmic loops from the transmembrane domains (e.g., Mourez et al., 1997)? Point mutations at residues believed to lie in or near the catalytic sites of CFTR's NBDs, chosen on the basis of the HisP and RbsA structures, should soon help resolve some of these questions (compare Vergani et al., 2000).

We thank Roberto Sánchez and Andrej Sali for help with alignments and for structural modeling, David Kopsco and Atsuko Horiuchi for technical assistance, and Kate Hall, Peter Hoff, and Paola Vergani for help with the manuscript and figures.

L. Csanády is a William O'Baker Graduate Fellow of The Rockefeller University. This work was supported by National Institutes of Health grant DK-51767.

Luis Reuss served as guest editor.

Submitted: 25 February 2000
Revised: 5 May 2000
Accepted: 5 June 2000

REFERENCES

Al-Nakkash, L., and T.-C. Hwang. 1999. Activation of wild-type and deltaF508-CFTR by phosphodiesterase inhibitors through cAMP-

dependent and -independent mechanisms. *Pflügers Arch.* 437: 553–561.

Annereau, J.-P., U. Wulbrand, A. Vankeerberghen, H. Cuppens, F. Bontems, B. Tümmler, J.-J. Cassiman, and V. Stoven. 1997. A novel model for the first nucleotide binding domain of the cystic fibrosis transmembrane conductance regulator. *FEBS Lett.* 407: 303–308.

Armstrong, S., L. Tabernero, H. Zhang, M. Hermodson, and C. Stauffacher. 1998. The 2.5 Å structure of the N-terminal ATP-binding cassette of the ribose ABC transporter. *Biophys. J.* 74: A338.

Bear, C.E., F. Duguay, A.L. Naismith, N. Kartner, H.W. Hanrahan, and J.R. Riordan. 1991. Cl^- channel activity in *Xenopus* oocytes expressing the cystic fibrosis gene. *J. Biol. Chem.* 266:19142–19145.

Berkower, C., and S. Michaelis. 1991. Mutational analysis of the yeast a-factor transporter STE6, a member of the ATP binding cassette (ABC) protein superfamily. *EMBO (Eur. Mol. Biol. Organ.) J.* 10:3777–3785.

Berkower, C., D. Taglicht, and S. Michaelis. 1996. Functional and physical interactions between partial molecules of STE6, a yeast ATP-binding cassette protein. *J. Biol. Chem.* 271:22983–22989.

Bibi, E., and H.R. Kaback. 1990. *In vivo* expression of the *lacY* gene in two segments leads to functional *lac* permease. *Proc. Natl. Acad. Sci. USA.* 87:4325–4329.

Betton, J.-M., and M. Hofnung. 1994. *In vivo* assembly of active maltose binding protein from independently exported protein fragments. *EMBO (Eur. Mol. Biol. Organ.) J.* 13:1226–1234.

Chan, K.W., L. Csanády, A.C. Nairn, and D.C. Gadsby. 1999. Deletion analysis of CFTR channel R domain using severed molecules. *Biophys. J.* 76:A405. (Abstr.)

Clancy, J.P., J.S. Hong, Z. Bebök, S.A. King, S. Demolombe, D.M. Bedwell, and E.J. Sorscher. 1998. Cystic fibrosis transmembrane conductance regulator (CFTR) nucleotide-binding domain 1 (NBD-1) and CFTR truncated within NBD-1 target to the epithelial plasma membrane and increase anion permeability. *Biochemistry.* 37:15222–15230.

Csanády, L. 2000. Rapid kinetic analysis of multi-channel records by a simultaneous fit to all dwell-time histograms. *Biophys. J.* 78:785–799.

Csanády, L., K.W. Chan, B.B. Angel, A.C. Nairn, and D.C. Gadsby. 1998. R-domain serine 768, a negative regulator of CFTR chloride channel gating. *J. Gen. Physiol.* 112:26a–27a. (Abstr.)

Csanády, L., and D.C. Gadsby. 1999. CFTR channel gating: incremental progress in irreversible steps. *J. Gen. Physiol.* 114:49–53.

Devidas, S., H. Yue, and W.B. Guggino. 1998. The second half of the cystic fibrosis transmembrane conductance regulator forms a functional chloride channel. *J. Biol. Chem.* 273:29373–29380.

Dulhanty, A.M., and J.R. Riordan. 1994. Phosphorylation by cAMP-dependent protein kinase causes a conformational change in the R domain of the cystic fibrosis transmembrane conductance regulator. *Biochemistry.* 33:4072–4079.

Gadsby, D.C., and A.C. Nairn. 1999. Control of CFTR channel gating by phosphorylation and nucleotide hydrolysis. *Physiol. Rev.* 79:S77–S107.

Gao, M., D.W. Loe, C.E. Grant, S.P.C. Cole, and R.G. Deeley. 1996. Reconstitution of ATP-dependent leukotriene C_4 transport by co-expression of both half-molecules of human multidrug resistance protein in insect cells. *J. Biol. Chem.* 271:27782–27787.

Groves, J.D., L. Wang, and M.J.A. Tanner. 1998. Functional reassembly of the anion transport domain of human red cell band 3 (AE1) from multiple and non-complementary fragments. *FEBS Lett.* 433:223–227.

Hartman, J., Z. Huang, T.A. Rado, S. Peng, T. Jilling, D.D. Muccio, and E.J. Sorscher. 1992. Recombinant synthesis, purification, and nucleotide binding characteristics of the first nucleotide binding domain of the cystic fibrosis gene product. *J. Biol. Chem.* 267: 6455–6458.

Higgins, C.F. 1992. ABC transporters: from microorganisms to man. *Annu. Rev. Cell Biol.* 8:67–113.

Hung, L.-W., I.X. Wang, K. Nikaido, P.-Q. Liu, G.F. Ames, and S.-H. Kim. 1998. Crystal structure of the ATP-binding subunit of an ABC transporter. *Nature.* 396:703–707.

Ishihara, H., and M.J. Welsh. 1997. Block by MOPS reveals a conformation change in the CFTR pore produced by ATP hydrolysis. *Am. J. Physiol. Cell Physiol.* 273:C1278–C1289.

Jones, P.M., and A.M. George. 1999. Subunit interactions in ABC transporters: towards a functional architecture. *FEMS (Fed. Eur. Microbiol. Soc.) Microbiol. Lett.* 179:187–202.

Kaczmarek, L.Y., U.R. Jennings, F. Strumwasser, A.C. Nairn, U. Walter, F.D. Wilson, and P. Greengard. 1980. Microinjection of catalytic subunit of cyclic AMP-dependent protein kinase enhances calcium action potentials of bag cell neurons in cell culture. *Proc. Natl. Acad. Sci. USA.* 77:7487–7491.

Ko, Y.H., M. Delannoy, and P.L. Pedersen. 1997. Cystic fibrosis transmembrane conductance regulator: the first nucleotide binding fold targets the membrane with retention of its ATP binding function. *Biochemistry.* 36:5053–5064.

Ko, Y.H., and P.L. Pedersen. 1995. The first nucleotide binding fold of the cystic fibrosis transmembrane conductance regulator can function as an active ATPase. *J. Biol. Chem.* 270:22093–22096.

Liman, E.R., J. Tytgat, and P. Hess. 1992. Subunit stoichiometry of a mammalian K^+ channel determined by construction of multimeric cDNAs. *Neuron* 9:861–871.

Loo, T.W., and D.M. Clarke. 1994. Reconstitution of drug-stimulated ATPase activity following co-expression of each half of human P-glycoprotein as separate polypeptides. *J. Biol. Chem.* 269: 7750–7755.

Mourez, M., M. Hofnung, and E. Dassa. 1997. Subunit interactions in ABC transporters: a conserved sequence in hydrophobic membrane proteins of periplasmic permeases defines an important site of interaction with the ATPase subunits. 1997. *EMBO (Eur. Mol. Biol. Organ.) J.* 16:3066–3077.

Moyer, B.D., J. Loffing, E.M. Schwiebert, D. Loffing-Cueni, P.A. Halpin, K.H. Karlson, I.I. Ismailov, W.B. Guggino, G.M. Langford, and B.A. Stanton. 1998. Membrane trafficking of the cystic fibrosis gene product, cystic fibrosis transmembrane conductance regulator, tagged with green fluorescent protein in Madin-Darby canine kidney cells. *J. Biol. Chem.* 273:21759–21768.

Naren, A.P., E. Cormet-Boyaka, J. Fu, M. Villain, J.E. Blalock, M.W. Quick, and K.L. Kirk. 1999. CFTR chloride channel regulation by an interdomain interaction. *Science.* 286:544–548.

Ostedgaard, L.S., D.P. Rich, L.G. DeBerg, and M.J. Welsh. 1997. Association of domains within the cystic fibrosis transmembrane conductance regulator. *Biochemistry.* 36:1287–1294.

Picciotto, M., J. Cohn, G. Bertuzzi, P. Greengard, and A.C. Nairn. 1992. Phosphorylation of the cystic fibrosis transmembrane conductance regulator. *J. Biol. Chem.* 267:12742–12752.

Ramjeesingh, M., C. Li, E. Garami, L.J. Huan, K. Galley, Y. Wang, and C.E. Bear. 1999. Walker mutations reveal loose relationship between catalytic and channel-gating activities of purified CFTR (cystic fibrosis transmembrane conductance regulator). *Biochemistry.* 38:1463–1468.

Randak, C., P. Neth, E.A. Auerswald, I. Assfalg-Machleidt, A.A. Roscher, H.B. Hadorn, and W. Machleidt. 1996. A recombinant polypeptide model of the second predicted nucleotide binding fold of the cystic fibrosis transmembrane conductance regulator is a GTP-binding protein. *FEBS Lett.* 398:97–100.

Randak, C., P. Neth, E.A. Auerswald, C. Eckerskorn, I. Assfalg-Machleidt, and W. Machleidt. 1997. A recombinant polypeptide

model of the second nucleotide-binding fold of the cystic fibrosis transmembrane conductance regulator functions as an active ATPase, GTPase and adenylate kinase. *FEBS Lett*. 410:180–186.

Riordan, J.R., J.M. Rommens, B.S. Kerem, N. Alon, R. Rozmahel, Z. Grzelczak, J. Zielenski, S. Lok, N. Plavsic, J. Chou, et al. 1989. Identification of the cystic fibrosis gene: cloning and characterization of complementary DNA. *Science*. 245:1066–1073.

Sheppard, D.N., L.S. Ostedgaard, D.P. Rich, and M.J. Welsh. 1994. The amino-terminal portion of CFTR forms a regulated Cl^- channel. *Cell*. 76:1091–1098.

Sheppard, D.N., and M.J. Welsh. 1999. Structure and function of the CFTR chloride channel. *Physiol. Rev*. 79:S23–S45.

Shiba, K., and P. Schimmel. 1992. Functional assembly of a randomly cleaved protein. *Proc. Natl. Acad. Sci. USA*. 89:1880–1884.

Shyamala, V., V. Baichwal, E. Beall, and G.F. Ames. 1991. Structure–function analysis of the histidine permease and comparison with cystic fibrosis mutations. *J. Biol. Chem*. 266:18714–18719.

Smit, L.S., D.J. Wilkinson, M.K. Mansoura, F.S. Collins, and D.C. Dawson. 1993. Functional roles of the nucleotide-binding folds in the activation of the cystic fibrosis transmembrane conductance regulator. *Proc. Natl. Acad. Sci. USA*. 90:9963–9967.

Stühmer, W., F. Conti, H. Suzuki, X. Wang, M. Noda, N. Yahagi, H. Kubo, and S. Numa. 1989. Structural parts involved in activation and inactivation of the sodium channel. *Nature*. 339:597–603.

Vergani, P., L. Csanády, C. Basso, R. Sanchez, A.C. Nairn, and D.C. Gadsby. 2000. Mutations near the predicted catalytic site of NBD1 affect CFTR Cl^- channel function surprisingly little. *Biophys. J*. 78:264A.

Walker, J.E., M. Saraste, M.J. Runswick, and N.J. Gay. 1982. Distantly related sequences in the α- and β-subunits of ATP synthase, myosin, kinases and other ATP-requiring enzymes and a common nucleotide binding fold. *EMBO (Eur. Mol. Biol. Organ.) J*. 8:945–951.

Wilkinson, D.J., M.K. Mansoura, P.Y. Watson, L.S. Smit, F.S. Collins, and D.C. Dawson. 1996. CFTR: the nucleotide binding folds regulate the accessibility and stability of the active state. *J. Gen. Physiol*. 107:103–119.

Yike, I., J. Ye, Y. Zhang, P. Manavalan, T.A. Gerken, and D.G. Dearborn. 1996. A recombinant peptide model of the first nucleotide-binding fold of the cystic fibrosis transmembrane conductance regulator: comparison of wild-type and delta F508 mutant forms. *Prot. Sci*. 5:89–97.

Zeltwanger, S., F. Wang, G.T. Wang, K.D. Gillis, and T.-C. Hwang. 1999. Gating of cystic fibrosis transmembrane conductance regulator chloride channels by adenosine triphosphate hydrolysis. *J. Gen. Physiol*. 113:541–554.